Bioorganic Chemistry 88 (2019) 102944

Contents lists available at ScienceDirect

Bioorganic Chemistry

journal homepage: www.elsevier.com/locate/bioorg

Design, synthesis and anticancer evaluation of thieno[2,3-*d*]pyrimidine derivatives as dual EGFR/HER2 inhibitors and apoptosis inducers

Souad A. Elmetwally[a], Khaled F. Saied[b,*], Ibrahim H. Eissa[c], Eslam B. Elkaeed[d,*]

[a] Department of Basic Science, Higher Technological Institute, 10th of Ramadan City 228, Egypt
[b] Department of Basic Science, Oral and Dental Medicine, Nahda University, East Beni-Suef, 62511 Beni-Suef, Egypt
[c] Department of Pharmaceutical Chemistry, Faculty of Pharmacy (Boys), Al-Azhar University, Nasr City, 11884 Cairo, Egypt
[d] Department of Pharmaceutical Organic Chemistry, Faculty of Pharmacy (Boys), Al-Azhar University, Nasr City, 11884 Cairo, Egypt

ARTICLE INFO

InChIKey:
XHUNEBYCLMLWHE-UHFFFAOYSA-N
Keywords:
Anticancer
Apoptosis
EGFR-TK
$EGFR^{WT}$
$EGFR^{T790M}$
HER2
Docking
Thieno[2,3-*d*]pyrimidine

ABSTRACT

Deregulation of many kinases is directly linked to cancer development and the tyrosine kinase family is one of the most important targets in current cancer therapy regimens. In this study, we have designed and synthesized a series of thieno[2,3-*d*]pyrimidine derivatives as an EGFR and HER2 tyrosine kinase inhibitors. All the synthesized compounds were evaluated *in vitro* for their inhibitory activities against $EGFR^{WT}$; and the most active compounds that showed promising IC_{50} values against $EGFR^{WT}$ were tested *in vitro* for their inhibitory activities against mutant $EGFR^{T790M}$ and HER2 kinases. Moreover, the antitumor activities of these compounds were tested against four cancer cell lines (HepG2, HCT-116, MCF-7 and A431). Compounds **13g**, **13h** and **13k** exhibited the highest activities against the examined cell lines with IC_{50} values ranging from 7.592 ± 0.32 to 16.006 ± 0.58 μM comparable to that of erlotinib (IC_{50} ranging from 4.99 ± 0.09 to 13.914 ± 0.36 μM). Furthermore, the most potent antitumor agent (**13k**) was selected for further studies to determine its effect on the cell cycle progression and apoptosis in MCF-7 cell line. The results indicated that this compound arrests G_2/M phase of the cell cycle and it is a good apoptotic agent. Finally, molecular docking studies showed a good binding pattern of the synthesized compounds with the prospective target, $EGFR^{WT}$ and $EGFR^{T790M}$.

1. Introduction

Cancer is a highly aggressive and lethal disease represents one of the greatest medical challenges in both more and less economic countries. According to the WHO fact sheet, published in September 2018 [1], cancer is classified as the second leading cause of death worldwide: it accounted for 9.6 million deaths in 2018. Mortality from cancer are projected to continue rising worldwide, with an estimated 13 million deaths in 2030. Cancer is caused by gene mutations or interfering with normal cell differentiation which initiated by drugs, viruses, smoking or diet [2].

Receptor tyrosine kinases (RTKs) are classes of signaling proteins which appear to be targeted more frequently by oncogenic mutations [3]. These enzymes catalyze the transfer of the γ-phosphate from ATP to tyrosine residues of its intracellular substrate and regulate the majority of cellular pathways [4], especially those involved in cell growth, proliferation, survival, metabolism, differentiation and apoptosis. Disruption of cell signaling cascades through kinase alterations (specially mutations, hyper-activation or hyper-production) leads to several diseases includes cancer [5–7], neurological disorders [8], inflammation [9], diabetes [10], autoimmune and cardiovascular disorders [11].

Epidermal growth factor receptor (EGFR) is a principal subfamily of the protein kinases, also called ErbB or HER receptors, that consists of four members: EGFR (ErbB1, HER1), ErbB2 (HER2), ErbB3 (HER3) and ErbB4 (HER4). EGFR is a key mediator playing a very important role in the regulation of fundamental cellular processes including: proliferation, survival as well as migration [12,13]. EGFR overexpression is one of the most extensively studied for its role in development of many human solid tumors as non-small cell lung cancer (NSCLC) [14], hepatocellular carcinoma (HCC) [15] and breast cancer [16]. Novel molecular strategies designed to target specific molecules affecting regulatory mechanisms involved in the control of cancer cell proliferation enable to improve cancer therapy efficiency compared to conventional chemotherapy and/or radiotherapy protocols. The aim of targeted

* Corresponding authors at: Department of Pharmaceutical Organic Chemistry, Faculty of Pharmacy (Boys), Al-Azhar University, Nasr City, 11884 Cairo, Egypt (E.B. Elkaeed).
E-mail addresses: soad.abdelaziz@hti.edu.eg (S.A. Elmetwally), khaled.saied@nub.edu.eg (K.F. Saied), Ibrahimeissa@azhar.edu.eg (I.H. Eissa), eslamkaeed@azhar.edu.eg (E.B. Elkaeed).

https://doi.org/10.1016/j.bioorg.2019.102944
Received 20 November 2018; Received in revised form 20 March 2019; Accepted 20 April 2019
Available online 25 April 2019

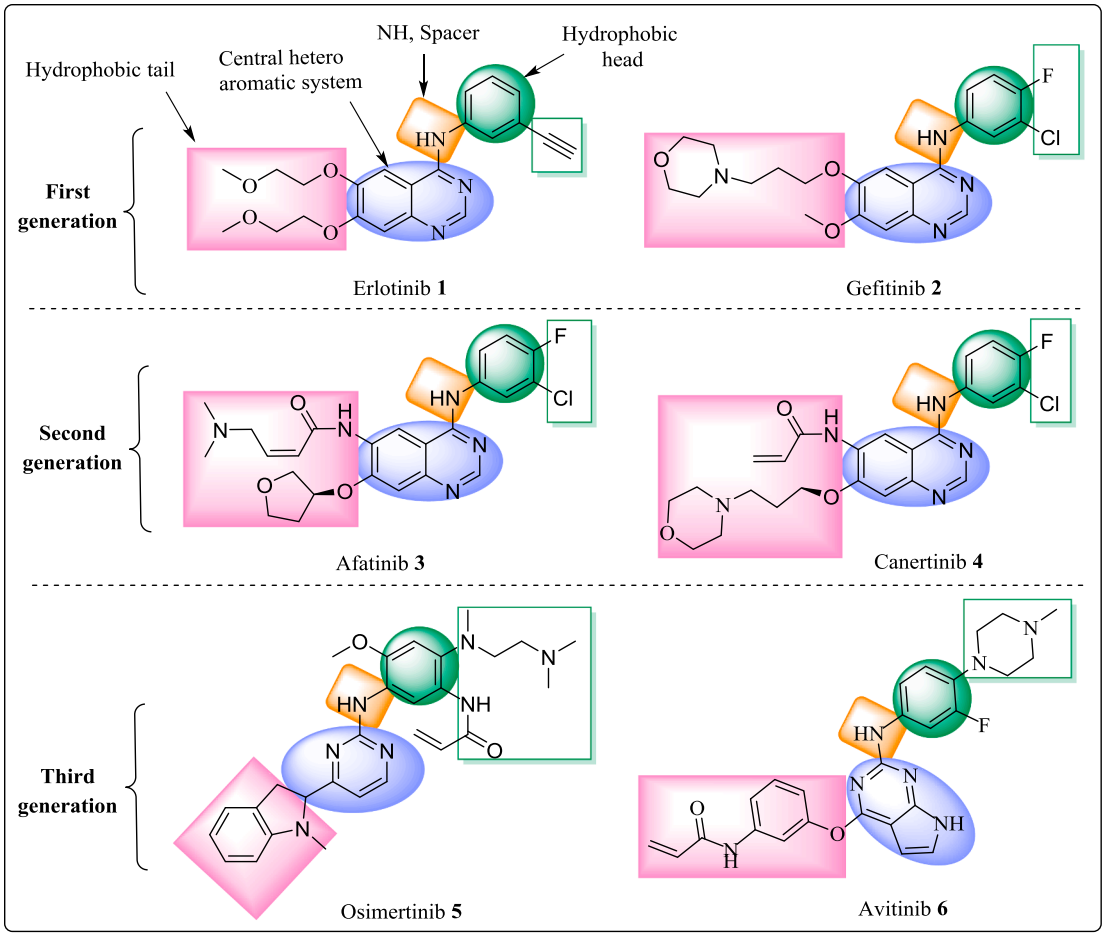

Fig. 1. Basic pharmacophoric features of EGFR-TK inhibitors.

therapies is inhibition and down-regulation or inactivation of over-active proteins responsible for triggering of aberrant cellular pathways [17–20].

HER2 is another member of the human epidermal growth factor receptor family which has a similar structure to EGFR [21]. Over-expression of this oncogene plays an important role in the progression of certain aggressive types of cancer [22].

Due to the vital role of overactive EGFR and HER2 tyrosine kinases as an important hallmarks of different types of cancer, such as lung cancer, colorectal cancer, pancreatic cancer, and head and neck cancer; inhibition of EGFR and HER2 pathway is a well-known target for effective anticancer therapies [22–27].

First generation of EGFR inhibitors are small molecules tyrosine kinase inhibitors (TKIs) such as erlotinib [28] **1** and gefitinib [29] **2**; they bind to the adenosine triphosphate (ATP)-binding site of the receptor, inhibiting intracellular tyrosine kinase domain (TKD) of the receptor. Both compounds have been used in the clinic to some success. However, only stabilizing effects of up to 12 months could be achieved. Although the overall response to EGFR-TKIs is high for patients with EGFR mutations, almost all patients subsequently develop acquired resistance to gefitinib and erlotinib within 10–16 months [30]. Due to the sobering performance of first generation EGFR inhibitors in the clinic, considerable effort has been put in the development of alternative approaches, resulting in second generation EGFR inhibitors; afatinib [31] **3** and canertinib [32] **4** were shown to effectively overcome EGFR-TK mutation-related resistance in *vivo* and xenograft models [33] and subsequently used successfully in clinical trials [34]. Unfortunately, they failed to meet endpoints against EGFR-mutant lung adenocarcinoma in clinical trials due to the limited therapeutic window offered by these agents [35,36]. As such, third generation EGFR-TKIs were developed: osimertinib **5** and avitinib **6** are irreversible EGFR-TKIs with a puckered ring structure that can bind the TKD active site in the presence of mutant EGFR [37–39]. These agents have been proven to be active in patients [40,41], and one of them, osimertinib, is FDA approved in 2015 to treat NSCLC. However, resistance to osimertinib is emerging [42], suggesting that alternative strategies and/or EGFR-TKIs are needed [43] (Fig. 1).

Thieno[2,3-*d*]pyrimidine nucleus is an important pharmacophore, presented in a number of anticancer agents [44–59], including EGFR and HER2-TKIs [44–46,59,60]. Compound **7** was designed and synthesized by Chia-Hsien Wu et al., using knowledge-based design strategy for ATP-competitive inhibitors interacting with the active site of the EGFR-TK. This compound showed low nanomolar efficacy for inhibiting the targeted enzyme, EGFR-TK [61]. Recently, another group, Milik et al., reported a new compound, **8**, as another example of thieno[2, 3-*d*]pyrimidines with anti EGFR and HER2-TK activity, having IC_{50} value of 13.9 μM against the NCI-H1975 cell line [59] (Fig. 2).

Based on the previous researches and attractiveness of tyrosine kinases as promising targets for the design of new cancer agents, it was decided to introduce new thieno[2,3-*d*]pyrimidine derivatives having inhibitory activities against wild-type EGFR-TK ($EGFR^{WT}$). All the compounds were tested against $EGFR^{WT}$ enzyme and also screened for their anti-proliferative activities against a number of cancer cell lines. The most active compounds were further tested against the mutated $EGFR^{T790M}$ and HER2 kinase. Moreover, the most active compound **13k** was investigated for its apoptosis induction potential in MCF-7 cell line. The cell phase which may be arrested by compound **13k** was

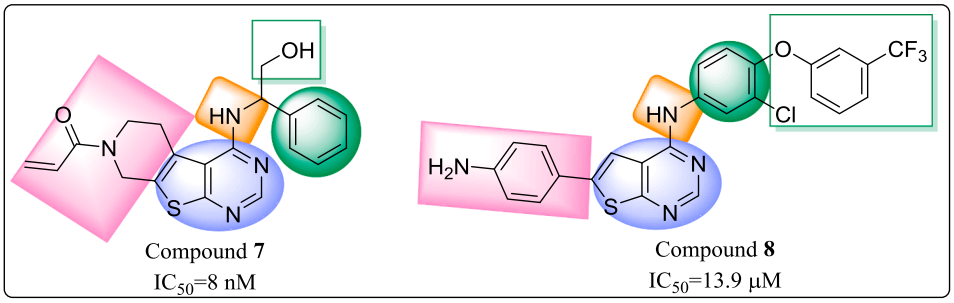

Fig. 2. Reported thieno[2, 3-*d*]pyrimidine derivatives as anti EGFR compounds.

determined by cell cycle assay. Finally, inhibitor molecular docking study, utilizing the crystal structure of EGFR kinase domain, of the active compounds was performed to investigate their binding patterns with the potential $EGFR^{WT}$ and $EGFR^{T790M}$ target.

1.1. Rational drug design

EGFR-TK domains consist of two lobes (or subdomains): The N-terminal and the C-terminal lobes. The lobes are connected by a short polypeptide chain, which is known as the linker, or the hinge region [62]. The ATP-EGFR binding site is divided into several distinct regions, although all these together form one space suitable for inhibitor binding; Adenine binding site/linker region, ribose binding pocket, phosphate binding pocket, back hydrophobic region and front hydrophobic region (Fig. 3) [62,63].

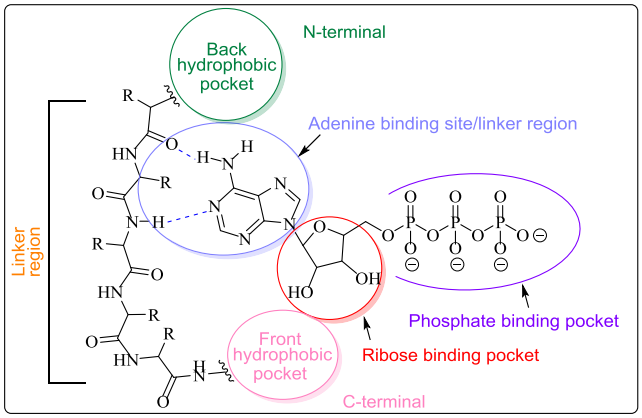

Fig. 3. Pharmacophore model of the ATP-binding site of EGFR-TK.

The linker region lies in the cleft at the junction of the N- and C-terminal lobes and it is a key section of the ATP nucleotide binding site – the adenosine moiety of ATP interacts via hydrogen bonds with the main chain of the linker region, and the rest interacts with glycine-rich, phosphate binding loop.

In principle, many properly substituted (heterocyclic) moieties that can interact with the ATP-binding site of an enzyme can serve as cores of kinase inhibitor. Among a number of different 5,6-heterocyclic systems, the thieno[2,3-*d*]pyrimidine core proved particularly suitable for the development of kinase inhibitors. Therefore, our goal was to synthesize several thieno[2,3-*d*]pyrimidine sub-series having the same essential pharmacophoric features of the reported and clinically used EGFR-TKIs as erlotinib **1** (Fig. 4). The core of our molecular design rational comprised bio-isosteric modification strategies of EGFR-TKIs at four different positions (Fig. 5).

The first position was the hetero aromatic ring system, where the thieno[2,3-*d*]pyrimidine nucleus was used as a bio-isostere for quinazoline moiety of erlotinib **1**. The choice of this moiety was based on an important bio-isosteric considerations. First of all, the bicyclic structure of thieno[2,3-*d*]pyrimidine core is convenient to the large size space of the adenine binding region [64]. Moreover, the heterocyclic nitrogen atoms serve as hydrogen-bond acceptors conferring excellent EGFR-TK potency [63]. The second position was the terminal hydrophobic head. Different hydrophobic moieties including (substituted) phenyl, aromatic, and fused aromatic heterocyclic structures were selected. The third position was the linker (spacer) region, where the linker length as well as number of its hydrogen acceptor and/or hydrogen acceptor groups were modified. The different linkers may be NH– as compounds **13a-i**, cyclic structure (e.g. NHPhNH) as compound **13j** and NHNH– as compound **13k**. The fourth position was the hydrophobic tail. Fused cyclohexyl group was incorporated at position-2,3-*d* of thienopyrimidine nucleus to occupy the front hydrophobic region of ATP binding site. All modification pathways and molecular design rationale were illustrated and summarized in Fig. 5.

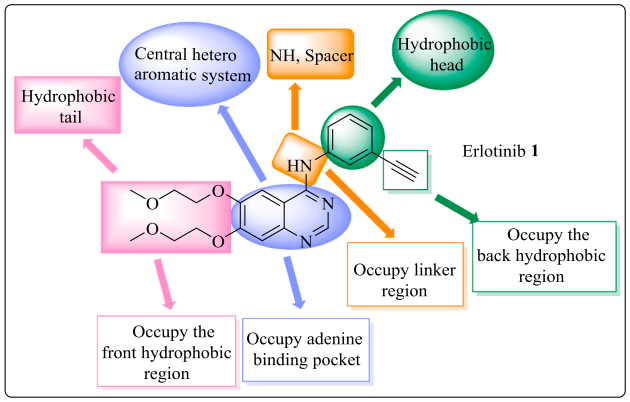

Fig. 4. The basic structural requirements for erlotinib as reported EGFR-TK inhibitor.

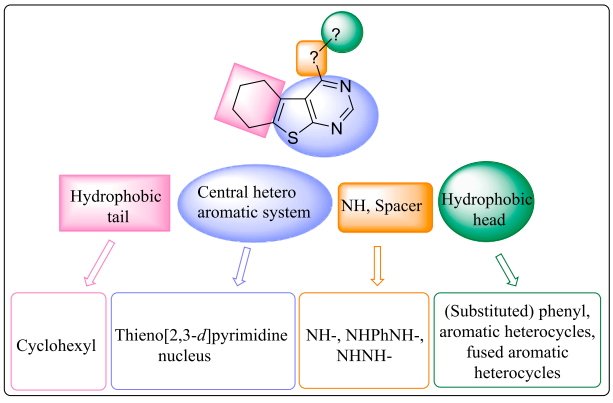

Fig. 5. Rational of molecular design of the new proposed EGFR-TK inhibitors.

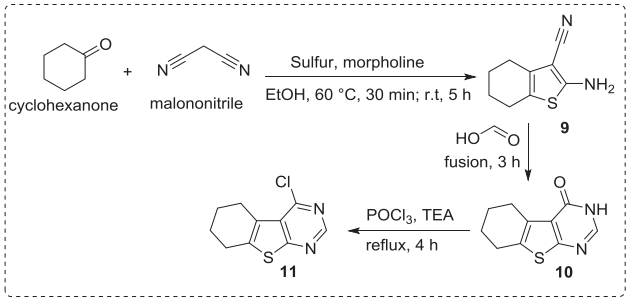

Scheme 1. Synthesis of compound **11**.

2. Results and discussion

2.1. Chemistry

According to the rational drug design, a series of thieno[2,3-*d*] pyrimidine scaffold was synthesized as outlined in Schemes 1–5. 2-Amino-4,5,6,7-tetrahydrobenzo[*b*]thiophene-3-carbonitrile (**9**), is the key intermediate for the synthesis of thieno[2,3-*d*]pyrimidines, which can be synthesized according to the reported methodology [65], by the condensation of commercially available cyclohexanone with malononitrile and sulphur powder using morpholine as catalyst. Fusion of compound **9** with formic acid afforded 5,6,7,8-tetrahydrobenzo[4,5] thieno[2,3-*d*]pyrimidin-4-one (**10**). Chlorination of **10** with $POCl_3$ yielded 4-chloro derivative **11** (Scheme 1) which served as a facile intermediate for nucleophilic substitution reactions with amines, hydrazine hydrate, sodium azide and *N*-phenylthiourea to afford our target compounds.

A possible mechanism is speculated and described in Scheme 2. The first step is a Knoevenagel condensation of methylene-active nitrile with a α-methylene carbonyl component of cyclohexanone to produce an α-β-unsaturated nitrile intermediate mediated by morpholine, which is then thiolated at the γ-methylene group with sulfur powder. The sulfurated compound undergoes cyclization to form the thiophene product, followed by an aromatization rearrangement through proton transfer (P.T). Cyclization of compound **9** was achieved by fusion with formic acid in the presence of water molecule. The last rearrangement of the cyclized product regenerates the aromaticity and allows the formation of the desired product **10**.

Reaction of compound **11** with appropriate amines namely, 2-aminobenzoic acid, 2-chloroaniline, 4-nitroaniline, 4-methoxyaniline, 4-aminobenzoic acid, 1-(4-aminophenyl)ethan-1-one, 2-amino-5-iodobenzoic acid, 4-aminophenol, 2-amino-4,5,6,7-tetra-hydrobenzo[*b*] thiophene-3-carbonitrile, benzene-1,2-diamine, and 4-hydrazinyl-5,6,7,8-tetrahydrobenzo[4,5]thieno[2,3-*d*]pyrimidine (**12**), afforded the target thieno[2,3-*d*]pyrimidine derivatives **13a-k** respectively in 60–90% yield, as shown in Scheme 3. The IR spectra of these compounds demonstrated stretching bands around 3400 cm^{-1} corresponding to the NH group, and other bands ranging from 1655 to 1693 cm^{-1} corresponding to C═O groups in compounds **13a**, **13e**, **13f** and **13g**.

The 4-hydrazino derivative **12** was prepared by reaction of compound **11** with 1.1 equivalent of hydrazine hydrate at room temperature [66]; when half equivalent amount of hydrazine hydrate was used, pyrimidine **13k** product was formed (Scheme 4). The MS spectrum of this compound exhibited correct molecular ion peak at m/z = 408.

The 4-chloro derivative **11** was further cyclized into the higher polycyclic compounds, tetrazolo **14** and triazolo **15** derivatives by reaction with sodium azide and thiosemicarbazide respectively in acetic

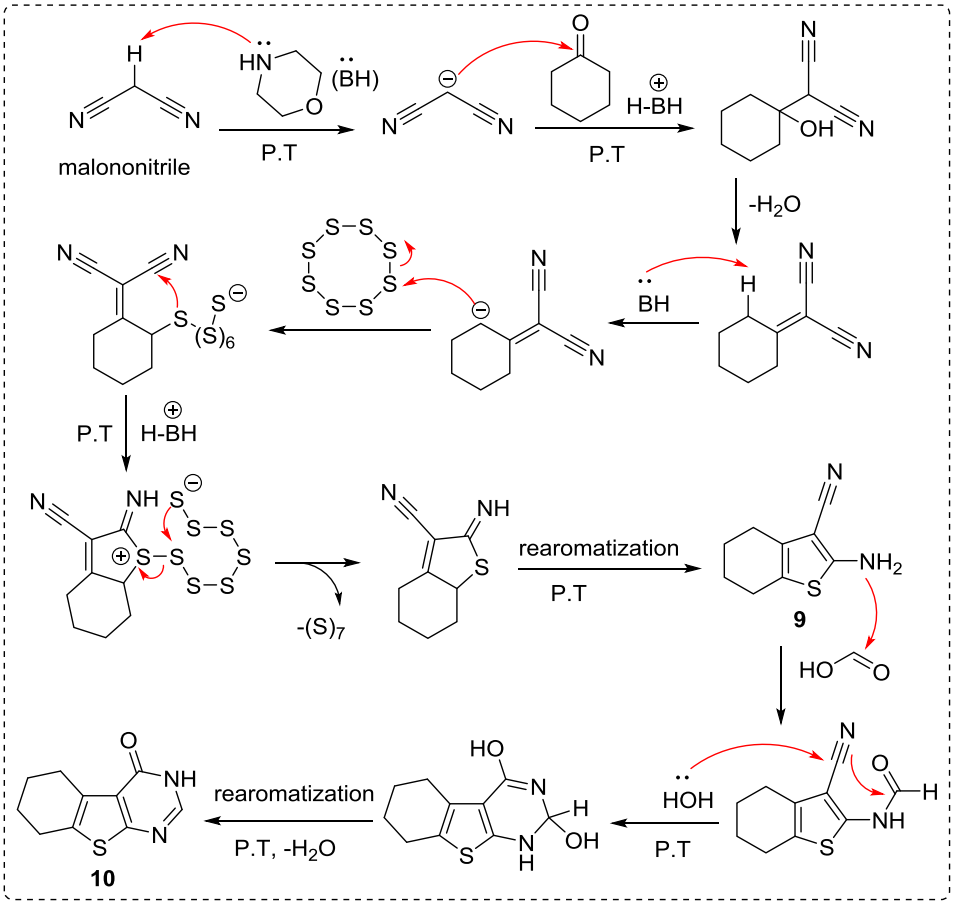

Scheme 2. Proposed reaction mechanism for compound **10** formation.

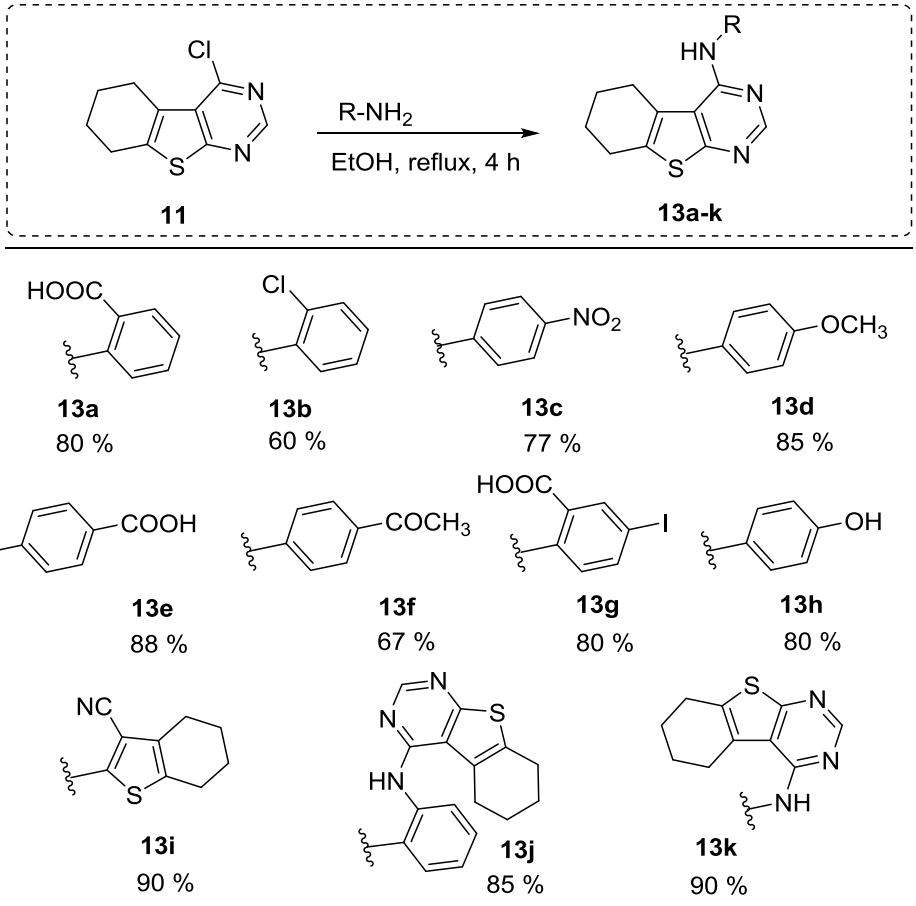

Scheme 3. Synthesis of compound **13a-k.**

acid [66], while the reaction with *N*-phenylthiourea yielded the unexpected 4-mercapto derivative **16** [67] instead of *N*-phenylthiourea derivative **17** (Scheme 5). Proposed mechanism for compound **16** formation is described in Scheme 6.

2.2. Biological evaluation

2.2.1. $EGFR^{WT}$, $EGFR^{T790M}$ and HER2 kinase inhibitory assay

Thirteen compounds were tested for their EGFR kinase inhibitory activities using EGFR Kinase Assay Kit (BPS biosciences). Erlotinib as one of the most potent $EGFR^{WT}$ inhibitors was used as a positive control. Most of the test compounds showed comparable inhibitory activities to erlotinib (0.387 μM) as shown in Table 1. The high reactivity of compound **13g** indicating that grafting a bulky iodo electron withdrawing substituent at the 4-position and carboxylic group at the 2-position of the phenyl ring may be beneficial for the activity; In addition, when the NH linker is extended by one more NH group as in compound **13k**, the yielded compound exhibited potent activity comparable to erlotinib. Further testing against the mutated $EGFR^{T790M}$ was done for compounds **13g**, **13h**, **13i** and **13k**. Compound **13k** was found to be the most active one against $EGFR^{T790M}$ comparable to erlotinib.

In addition to the inhibitory effect against EGFR kinase, the most active compounds were further evaluated for their selectivity against HER2 kinase using HER2 Kinase Assay Kit (BPS biosciences). Fortunately, compound **13k** have the strongest HER2 inhibitory effect with IC_{50} value of 0.415 μM.

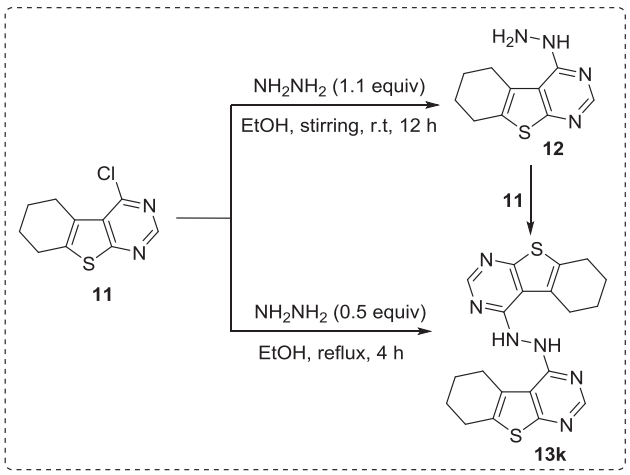

Scheme 4. Reaction of **11** with hydrazine hydrate.

2.2.2. In vitro anti-proliferative activities

The anti-proliferative activities of the synthesized compounds were evaluated against four cancer cell lines; hepatocellular carcinoma (HepG2), colon carcinoma (HCT-116), human breast adenocarcinoma (MCF-7) and human epithelial carcinoma (A431) using MTT assay [68]. These cancer cell lines have a high expression of EGFR [69–72]. The commercially available erlotinib was used in this test as a reference compound. As shown in Table 2, the obtained results revealed that the examined compounds showed versatile anti-proliferative activities against the tested cell lines. Compound **13g** showed IC_{50} near to the reference compound (erlotinib) in HCT-116 and A431 cells, while compound **13h** evidently reduced the viability of HCT-116 cells with IC_{50} of 10.14 ± 1.1 μM which was comparable to that of erlotinib (13.91 ± 0.36 μM). Also, in alignment with the inhibitory effects on

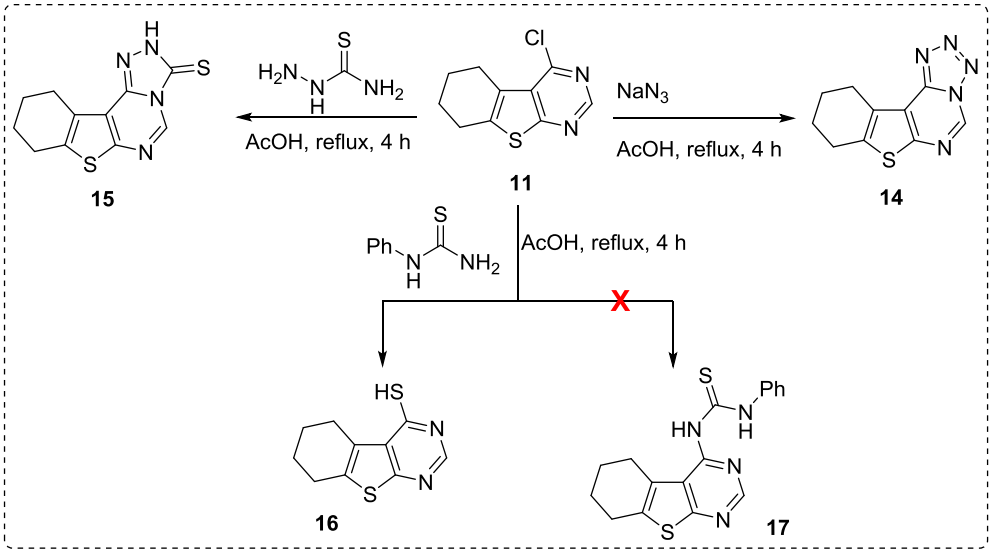

Scheme 5. Synthesis of compound **14**, **15** and **16.**

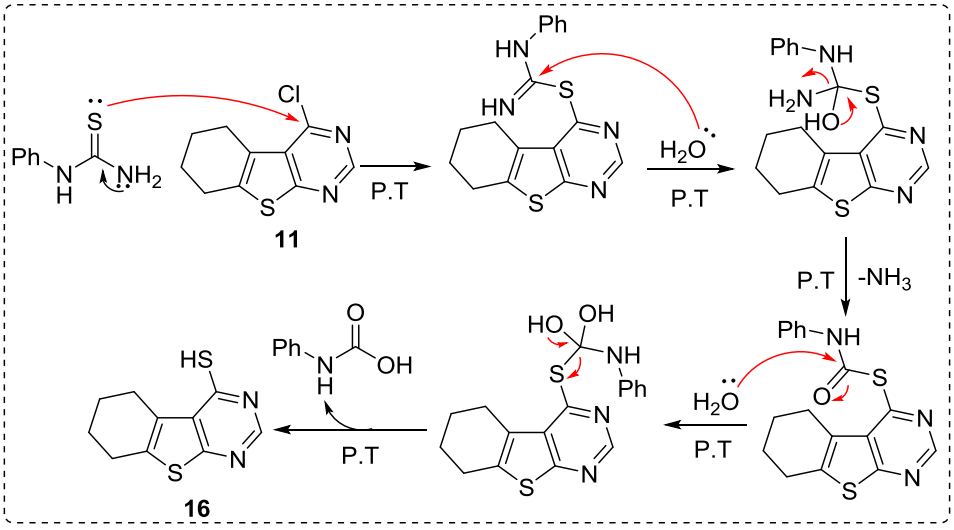

Scheme 6. Proposed reaction mechanism for compound **16** formation.

HCT-116, compound **13h** exhibited s strong cytotoxic effect against HepG2 with IC_{50} of 13.02 ± 1.00. Compound **13i** have a strong cytotoxic effect against A431 cells with IC_{50} of 13.77 ± 0.71. The most potent cytotoxic agent, compound **13k,** exhibit a significant activity against HepG2, MCF-7 and A431 cells with IC_{50} values of 7.975 ± 0.37, 7.592 ± 0.32 and 9.46 ± 0.44 μM, respectively. However, it showed a moderate activity against HCT-116. The rest of compounds (**11**, **13a-f, 13j** and **16**) didn't show promising cytotoxic activities as the mentioned compounds.

Table 1
In vitro enzymatic inhibitory activities of thieno[2,3-*d*]pyrimidines against $EGFR^{WT}$, $EGFR^{T790M}$ and HER2.

Comp.	$EGFR^{WT}$ IC_{50} (μM)	$EGFR^{T790M}$ IC_{50} (μM)	HER2 IC_{50} (μM)	Comp.	$EGFR^{WT}$ IC_{50} (μM)	$EGFR^{T790M}$ IC_{50} (μM)	HER2 IC_{50} (μM)
11	NT[a]	NT[a]	NT[a]	**13h**	0.630	0.956	0.858
12	0.560	NT[a]	NT[a]	**13i**	0.443	0.908	0.722
13a	0.865	NT[a]	NT[a]	**13j**	1.440	NT[a]	NT[a]
13b	NT[a]	NT[a]	NT[a]	**13k**	**0.278**	0.352	0.415
13c	0.459	NT[a]	NT[a]	**14**	NT[a]	NT[a]	NT[a]
13d	0.605	NT[a]	NT[a]	**15**	0.550	NT[a]	NT[a]
13e	0.488	NT[a]	NT[a]	**16**	0.475	NT[a]	NT[a]
13f	16.352	NT[a]	NT[a]	**Erlotinib**	0.387	0.241	0.117
13g	**0.174**	0.608	0.711				

Bold font indicates superior potency than erlotinib.
[a] NT: Compounds not tested.

Table 2
In vitro anti-proliferative activities towards HepG2, HCT-116, MCF-7 and A431 cell lines.

Compound	IC_{50} (μM)[a]			
	HepG2	HCT-116	MCF-7	A431
11	54.89 ± 3.10	58.05 ± 2.70	67.48 ± 3.20	NT[b]
12	NT[b]	NT[b]	NT[b]	NT[b]
13a	87.63 ± 4.30	71.82 ± 3.60	81.60 ± 3.90	NT[b]
13b	36.10 ± 2.20	40.03 ± 2.40	46.45 ± 2.50	NT[b]
13c	85.32 ± 4.10	64.06 ± 3.40	77.9 ± 3.60	NT[b]
13d	42.52 ± 2.50	26.26 ± 1.70	25.77 ± 1.80	NT[b]
13e	67.72 ± 3.70	62.57 ± 3.30	75.75 ± 3.40	NT[b]
13f	35.08 ± 1.90	50.73 ± 2.60	53.71 ± 3.10	NT[b]
13g	26.446 ± 1.33	**16.006 ± 0.58**	23.928 ± 1.44	16.14 ± 0.62
13h	**13.02 ± 1.00**	**10.14 ± 1.10**	12.68 ± 1.30	47.05 ± 1.29
13i	27.29 ± 1.60	30.18 ± 1.90	37.08 ± 2.00	13.77 ± 0.71
13j	70.92 ± 3.90	90.76 ± 4.30	95.34 ± 4.60	NT[b]
13k	**7.975 ± 0.37**	50.29 ± 2.71	**7.592 ± 0.32**	**9.46 ± 0.44**
14	NT[b]	NT[b]	NT[b]	NT[b]
15	NT[b]	NT[b]	NT[b]	NT[b]
16	20.39 ± 1.50	17.72 ± 1.40	17.39 ± 1.60	NT[b]
Erlotinib	6.733 ± 0.33	13.914 ± 0.36	3.107 ± 0.14	4.99 ± 0.09

Bold font indicates a high potency relative to erlotinib.

[a] IC_{50} values are the mean ± S.D. of three separate experiments; IC_{50} (μM): 1–10 (very strong), 11–20 (strong), 21–50 (moderate), 51–100 (weak), more than 100 (non-cytotoxic).

[b] NT: Compounds not tested for their anti-proliferative activities.

2.2.3. *In-vitro DNA-flow cytometric (cell cycle) analysis*

The most active compound **13k** was selected for further studies regarding its effect on cell cycle progression in the MCF-7 cell line. DMSO was used as a negative control. Cell cycle stages were being recognized through flow cytometry after propidium iodide (PI) staining followed by RNAse treatment. The MCF-7 cells were incubated with 1 μM of compound **13k** for 24 h. The flow cytometry was employed to quantify cell populations in different cell cycle phases (pre-G_1, G_1, S and G_2/M phases).

The results indicated that treating MCF-7 cells with compound **13k** resulted in an interference with the normal cell cycle distribution of this cell line. This compound induced a significant increase in the percentage of cells at phases of pre-G_1, which could be indicative of apoptosis, and G_2/M by 16.3 and 4.7 folds respectively, comparing to the control. Such increase was accompanied by a significant decrease in the percentage of cells at the G_1 and S-phase of the cell cycle. This result clearly indicated that compound **13k** arrests G_2/M phase of cell cycle (Figs. 6, 7 & Table 3).

2.2.4. *Determination and assay of apoptosis using Annexin V-FITC staining*

The mode of cell death induced by compound **13k** was further investigated to determine whether death is due to apoptosis or necrosis. This was elucidated using Annexin V/PI assay. Annexin V conjugated with FITC is used to stain cells in combination with PI. Cells that stained positive for Annexin V/PI represents the cells in the late apoptotic stage that have lost membrane integrity [73].

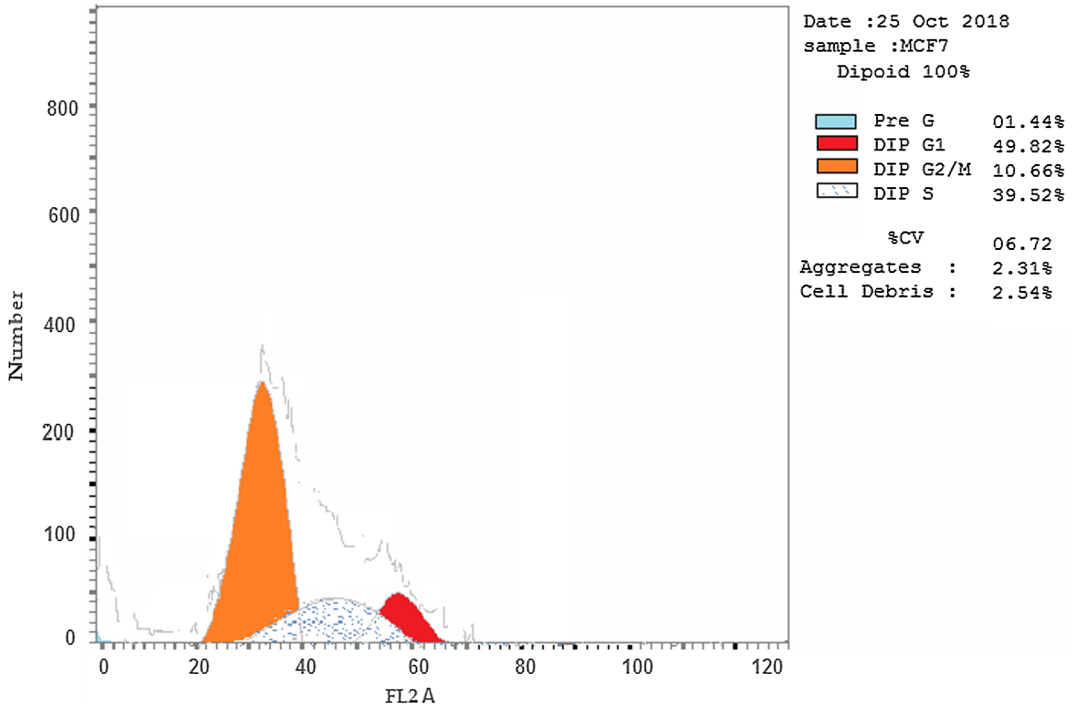

Fig. 6. Cell cycle analysis of MCF-7 cells treated with DMSO.

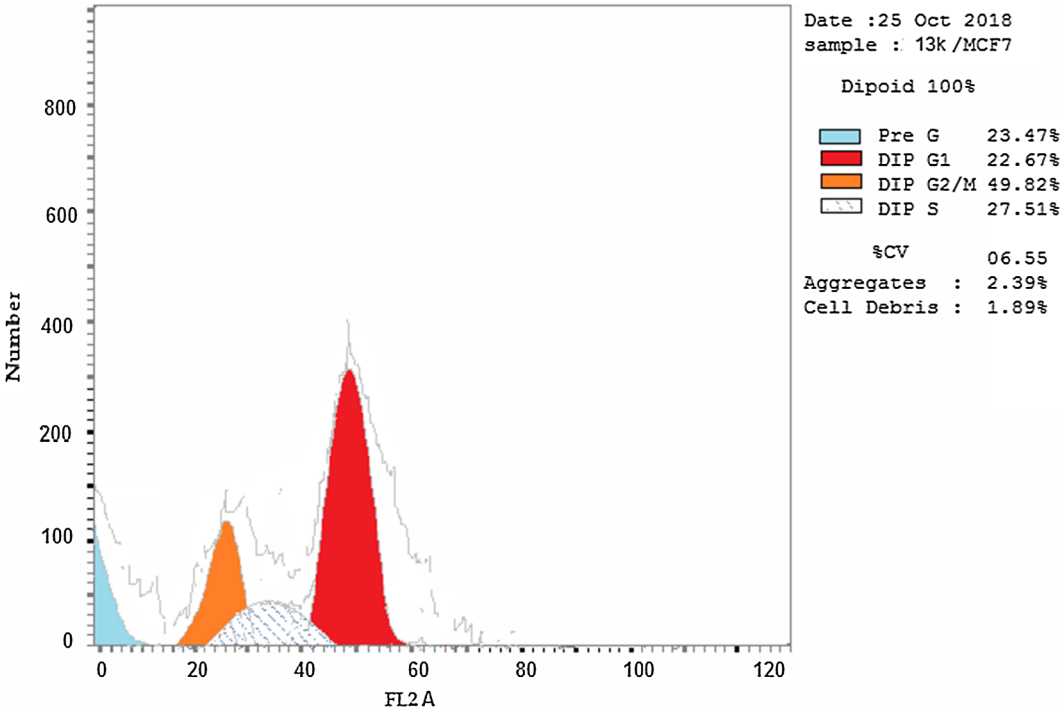

Fig. 7. Cell cycle analysis of MCF-7 cells treated with compound **13k** at 1 μM concentration.

As EGFR-TK inhibitors can induce cancer cell apoptosis [74], the apoptotic nature of compound **13k** against MCF-7 cells was evaluated via flow cytometry detection using AnnexinV-FITC and PI double staining. The representative dot plots of flow cytometric analyses of MCF-7 cells demonstrated four different distributions (Fig. 8): healthy cells (Lower Left; Annexin V and PI negative), cells in early apoptosis (Lower Right; Annexin V positive and PI negative), cells in late apoptosis (Upper Right; Annexin V and PI positive) and dead or necrotic cells (Upper Left; Annexin V negative and PI positive). The results shown in Fig. 8 and Table 4 revealed that application of compound **13k** on MCF-7 cells for 48 h with increasing its concentration from 0 μM to 1 μM, increases the early apoptosis ratio (lower right quadrant of the cytogram) from 0.72% to 7.92%, and increases the late apoptosis ratio (upper right quadrant of the cytogram) from 0.27% to 12.47%. This means that treating MCF-7 cells with compound **13k** resulted in a significant increase in the percentage of apoptotic cells compared to non-treated control. Additionally, a slight increase in the number of necrotic cells was seen. The total number of early and late apoptotic cells is higher compared to the number of necrotic cells, indicating that apoptosis is the main mechanism by which **13k** causes cell death.

2.3. Docking studies

Additionally, molecular modeling studies were performed in order to rationalize the anticancer activities of the proposed compounds. All the synthesized thieno[2,3-*d*]pyrimidine derivatives were subjected to docking study together with the internal ligand, erlotinib, as a reference molecule to explore their calculated binding modes with the EGFR wild type receptor ($EGFR^{WT}$, PDB: 4HJO) [75]. The ATP binding pocket of $EGFR^{WT}$ consists of five main parts; sugar pocket, two hydrophobic regions, adenine binding pocket, and phosphate binding region. The sugar pocket contains Cys773 residue, which is unique to the EGFR-TK and provides both potency and selectivity. The back hydrophobic region comprises Thr766, Lys721 and Thr830 residues, playing a crucial role in inhibitor selectivity. The front hydrophobic region is formed by Gly772 and Leu694 residues. The adenine region contains electrostatic interaction between the amino group of the adenine ring and Met769 residue. The phosphate binding region offers little opportunity in terms of inhibitor binding affinity due to high solvent exposure [63,76] (Fig. 9).

Table 3
Effect of compound **13k** and DMSO on cell cycle of MCF-7 cell line.

Sample data		Results				
Sample/cell line	Conc (μM)	% G_1	% S	% G_2/M	% Pre-G_1	Comment
13k/MCF-7	1	22.67	27.51	49.82	23.47	Cell growth arrest at G_2/M phase
DMSO/MCF-7	–	49.82	39.52	10.66	1.44	

The results of docking studies against the $EGFR^{WT}$ revealed that the synthesized compounds have similar orientations inside the ATP binding site. The designed compounds gave good binding energies ranging from −13.78 to −25.27 kcal/mol (Table 5). The binding mode of the co-crystallized ligand, erlotinib, exhibited an energy binding of −25.17 kcal/mol. Quinazoline nucleus was oriented in the adenine pocket of the receptor, forming a hydrogen bond (3.01 Å) between the N − 1 atom of pyrimidine ring and Met769, while the phenyl ring formed pi-sigma interaction with Lue694. The bis (2-methoxyethoxy) groups occupied the front hydrophobic region forming hydrophobic interaction with Gly772, Pro770 and Leu694 residues. Besides, the ethynyl phenyl moiety occupied the back hydrophobic pocket forming pi-cation interaction with Lys721, and hydrophobic interaction with Thr830, Lue764, Ala719 and Thr766 residues (Fig. 9). Further docking studies have been done for the most active compounds **13g-i** and **13k** against the mutated EGFR ($EGFR^{T790M}$, PDB: 3W2O); the docked compounds **13g-i** have almost similar binding free energy while the most active one, **13k**, has a binding free energy of −28.56 which is higher than that of erlotinib ligand (Table 5).

The binding mode of compound **13j** was higher than that of erlotinib, with affinity value of −25.27 kcal/mol. The thieno[2,3-*d*]pyrimidine moiety occupied the adenine binding site forming a hydrogen

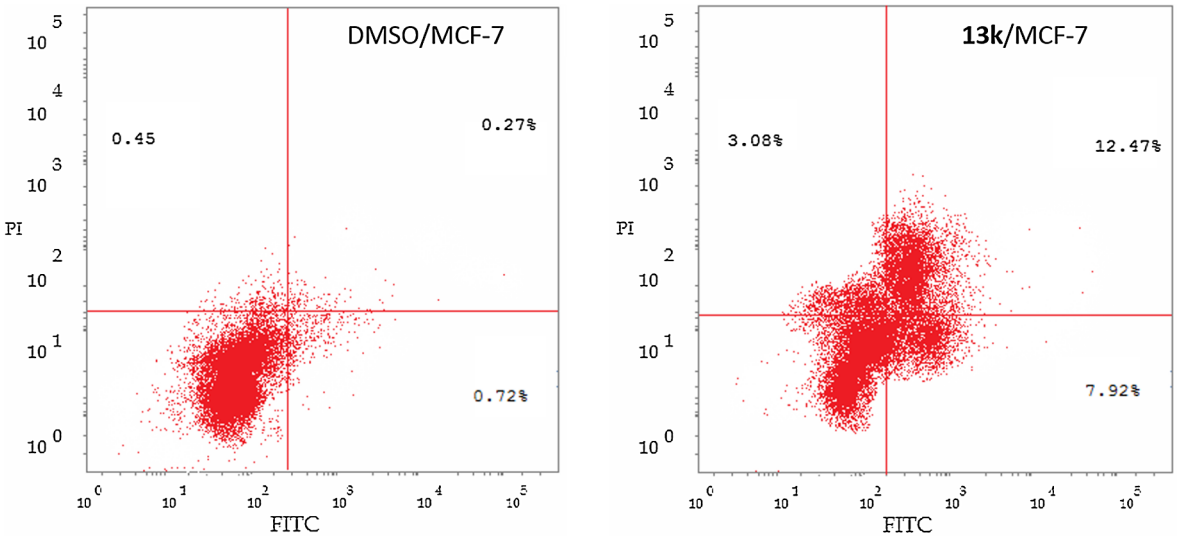

Fig. 8. Flow cytometry analysis of MCF-7 cell line treated with DMSO and compound **13k**.

Table 4
Effect of compound **13k** and DMSO on the percentage of annexin V-FITC-positive staining in MCF-7 cells.

Sample data		Apoptosis (%)			Necrosis (%)
Sample/cell line	Conc (μM)	Total	Early	Late	–
13k/MCF-7	1	23.47	7.92	12.47	3.08
DMSO/MCF-7	–	1.44	0.72	0.27	0.45

bond with Lys704 with a distance of 3.17 Å. The cyclohexyl moiety occupied the front hydrophobic pocket forming hydrophobic interactions with Phe771 and Pro770 residues. In addition, the central phenyl moiety of NH-Ph-NH linker forms hydrophobic interaction with Leu694, gly772 and Met769. Moreover, this linker length provides the other thieno[2,3-*d*]pyrimidine moiety higher flexibility to get closer to Val702, Arg817, Leu820 and Cys773 forming hydrophobic interaction in the back hydrophobic region (Fig. 10).

The binding mode of compound **13f** was as like as that of erlotinib, with affinity value of −24.84 kcal/mol. General hydrophobic interactions were seen between the adenine ring, cyclohexyl and phenyl moieties with Val702, Leu694, cys773, Thr830, Lys721 and Thr766 of the adenine and two hydrophobic pockets (Fig. 11).

Similar results were obtained for synthetic inhibitor **13h**. This compound showed an energy binding of −23.18 kcal/mol. An electrostatic interaction involving H-bond noted between the adenine N atom and water molecule binding to Thr766 and Thr830. The adenine and two hydrophobic binding pockets also showed varying interactions between the adenine ring with Ala 719/Leu820, cyclohexyl ring with Val702, and 4-OH phenyl with Leu719/Thr 830 (Fig. 12).

Compound **13k** has a binding energy nearly similar to that of erlotinib. Pyrimidine nucleus positioned closely towards Met-769 forming two hydrogen bonds with the N3 and the linker NH with a distance of 2.95 and 2.92 Å, respectively. On the other side of **13k**, a third hydrogen bond formed between the N1 and Lys704 with a shorter

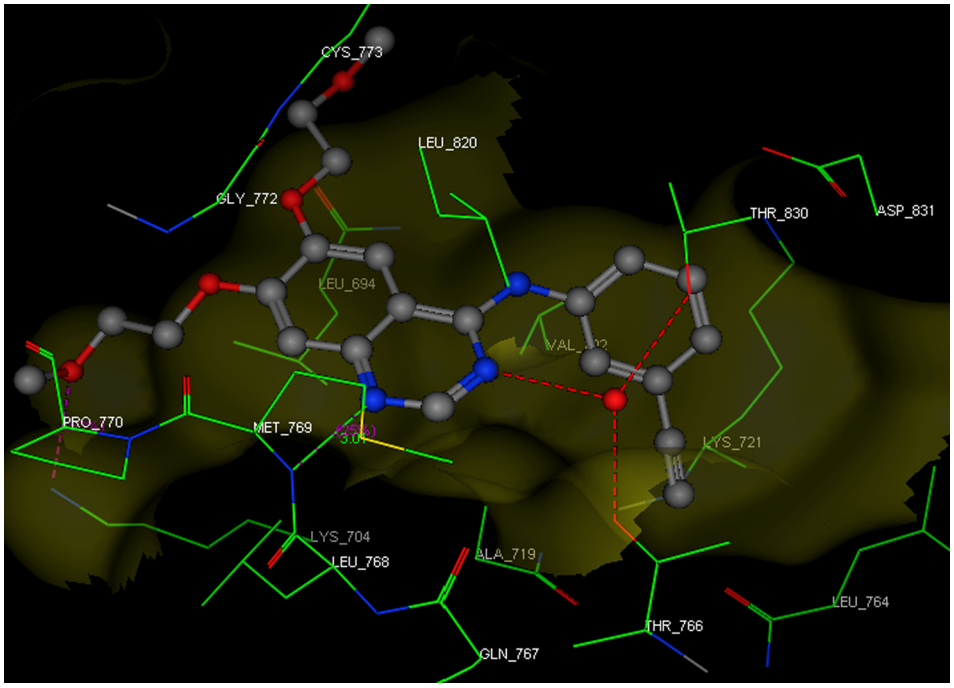

Fig. 9. Superposition of erlotinib (grey sticks) in the binding pocket of $EGFR^{WT}$ receptor (PDB ID code: 4HJO). The active pocket was represented as a yellow surface. The surrounding residues have been depicted as green sticks. (For interpretation of the references to colour in this figure legend, the reader is referred to the web version of this article.)

Table 5
The docking binding free energies of the synthesized compounds against $EGFR^{WT}$ and $EGFR^{T790M}$.

Compound	Binding free energy (kcal/mol)	
	$EGFR^{WT}$	$EGFR^{T790M}$
11	−14.04	–
12	−16.30	–
13a	−18.51	–
13b	−18.07	–
13c	−21.96	–
13d	−21.38	–
13e	−22.99	–
13f	−24.84	–
13g	−19.10	−21.78
13h	−23.18	−21.69
13i	−20.38	−21.92
13j	−25.27	–
13k	−22.11	−28.56
14	−14.64	–
15	−14.48	–
16	−13.78	–
Erlotinib	−24.87	−26.66

distance of 2.78 Å (Fig. 13). The binding mode of **13k** with the mutated $EGFR^{T790M}$, showed a hydrogen bond formed with Met793 with a distance of 3.21 Å (Fig. 14).

In general, most of the synthetic inhibitors have moderate to strong potency relative to the internal ligand, erlotinib.

3. Structure-activity relationships (SAR)

Observing the results of biological tests in Table 2, valuable data about the structure-activity relationships of thieno[2,3-*d*]pyrimidine derivatives as potential EGFR-TK inhibitors could be deduced in comparison to the tested standard inhibitor.

Initially, the effect of different linkers on the activity against $EGFR^{WT}$ was investigated. It was found that replacement of the NH linker with cyclic (NHPhNH-) linker in compound **13j** provide very weak inhibition activity (IC_{50} range = 70.92–95.34 μM), while compound **13k** with one more NH group in the linker was found to be strong cytotoxic inhibitor (IC_{50} range = 7.59–9.46 μM) in HepG2, MCF-7 and A431 cell lines. In absence of the linker and the hydrophobic head and replacement them by SH group in compound **16**, the growth inhibition of the cancer cell lines showed moderate activity (IC_{50} range = 17.39–20.39 μM).

The impact of the substitution on the phenyl group of terminal hydrophobic head was explored. The high activity of compound **13h** (IC_{50} range = 10.14–13.02 μM) may be attributed to the presence of 4-OH substituent as an electron donating group on the phenyl ring, however, replacement of 4-OH in compound **13h** by bulkier electron donating group (4-OCH_3) decreased the growth inhibition, like in the case of compound **13d**. The presence of electron withdrawing group such as 2-COOH in compounds **13a,g**, 2-Cl in **13b** and 4-NO_2 in **13c** decreased the growth inhibition activity.

Finally, more bulky hydrophobic head and the longer NHNH linker in **13k** dimer are capable of extending into the back pocket of the receptor forming three H-bonds, resulting in an effective HepG2, MCF-7 and A431 cell line growth inhibition.

4. Conclusion

In summary, sixteen thieno[2,3-*d*]pyrimidine derivatives (**11**, **12**, **13a-k**, **14**, **15** and **16**) were designed, synthesized and evaluated for their inhibitory activities against $EGFR^{WT}$, $EGFR^{T790M}$ and HER2 kinases. Compounds **13g** and **13k** showed excellent inhibitory activities. The tested compounds were further evaluated *in vitro* for their inhibitory action against four cancer cell lines (HepG2, HCT-116, MCF-7 and A431) and compared with erlotinib as a positive control. In this study, three of the synthesized compounds (**13g**, **13h** and **13k)** showed growth cell line inhibitory effect similar to standard control with IC_{50} values ranging from 7.592 ± 0.32 to 16.006 ± 0.58 μM. The SAR

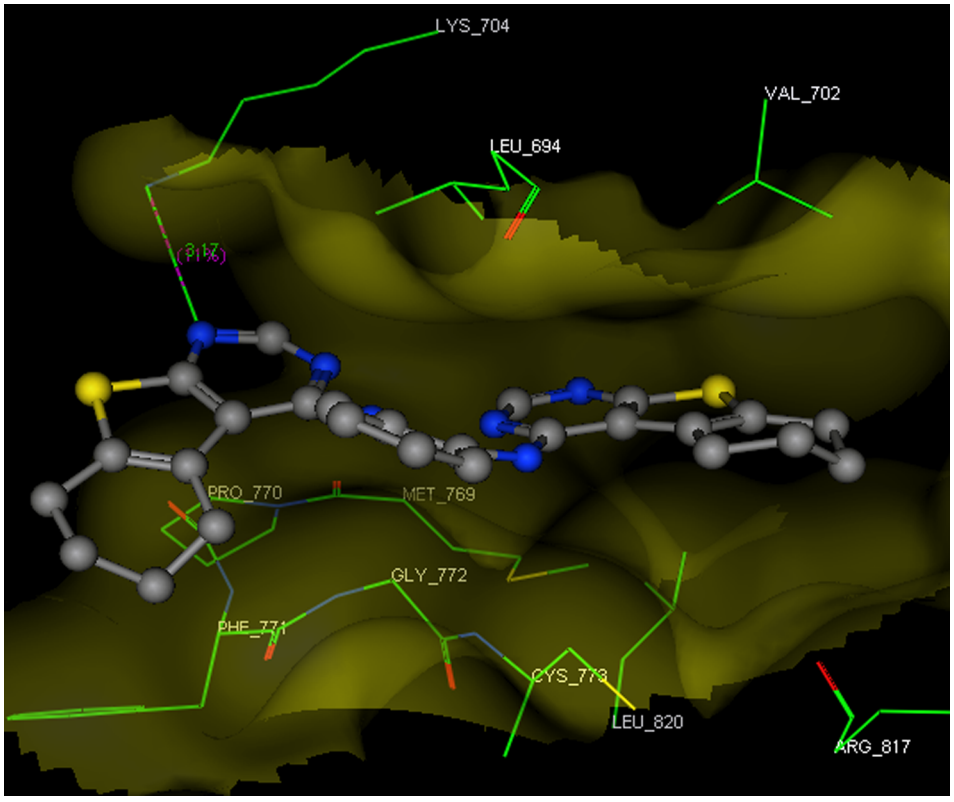

Fig. 10. Calculated binding mode of compound **13j** (grey sticks) within the binding pocket of $EGFR^{wt}$ receptor. The active pocket has been represented as yellow surface. Important binding sites residues have been depicted as green sticks; other residues have been hidden for sake of clarity. (For interpretation of the references to colour in this figure legend, the reader is referred to the web version of this article.)

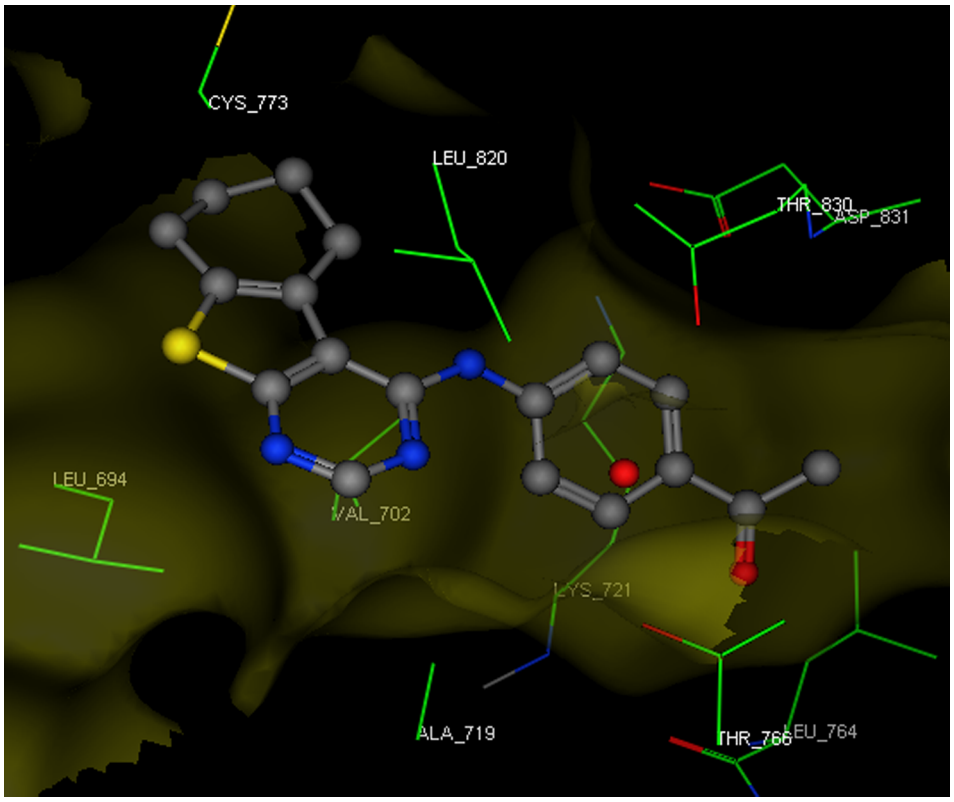

Fig. 11. Calculated binding mode of compound **13f** (grey sticks) within the binding pocket of $EGFR^{wt}$ receptor. The active pocket has been represented as yellow surface. Important binding sites residues have been depicted as green sticks. (For interpretation of the references to colour in this figure legend, the reader is referred to the web version of this article.)

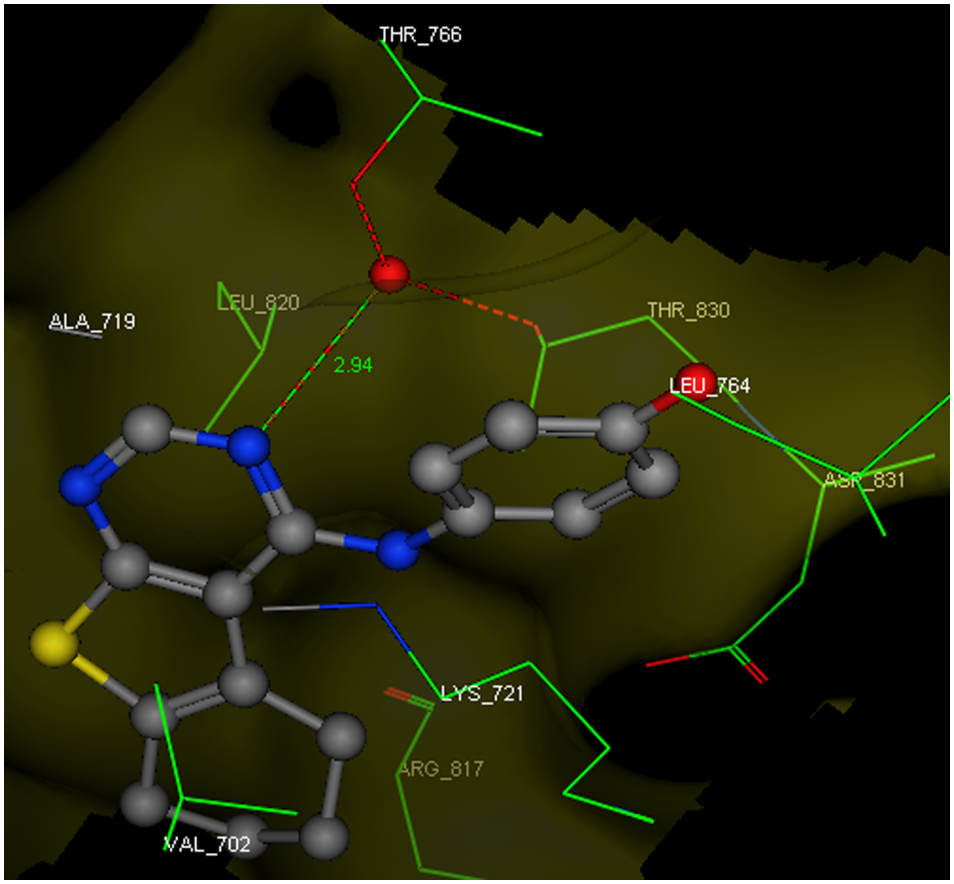

Fig. 12. Calculated binding mode of compound **13h** (grey sticks) within the binding pocket of $EGFR^{wt}$ receptor. The active pocket has been represented as yellow surface. Important binding sites residues have been depicted as green sticks. (For interpretation of the references to colour in this figure legend, the reader is referred to the web version of this article.)

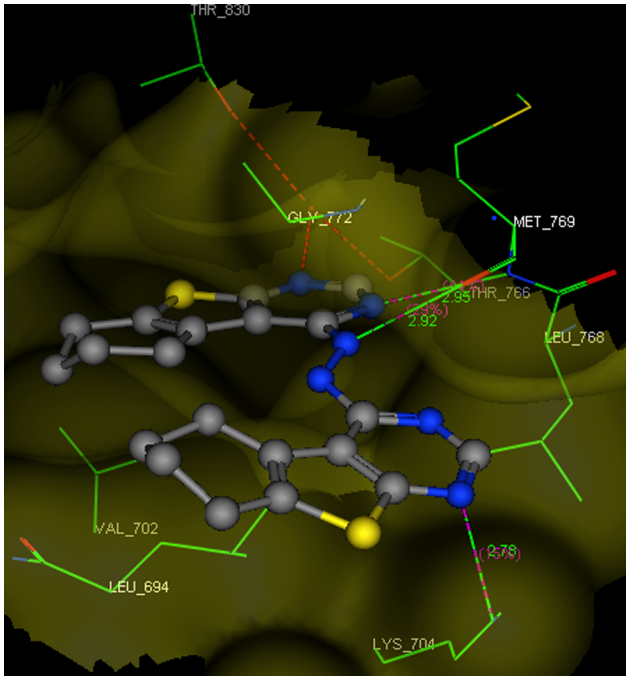

Fig. 13. Calculated binding mode of compound **13k** (grey sticks) within the binding pocket of EGFR^{wt} receptor. The active pocket has been represented as yellow surface. Important binding sites residues have been depicted as green sticks. (For interpretation of the references to colour in this figure legend, the reader is referred to the web version of this article.)

studies pointed that, the less bulky electron donating group substitution on the terminal hydrophobic head seems to be preferred. Also, it was found that a longer linker and bulky hydrophobic head in **13k** is advantageous. Further, compound **13k** was tested for its effect on cell cycle progression and induction of apoptosis in the MCF-7 cell line. It was found that it has an apoptotic effect and can arrest G_2/M phase of cell cycle. Also, molecular docking studies was carried out to recognize the binding pattern of the synthesized compounds against EGFR^{WT} and EGFR^{T790M} receptor. Most of the synthesized compounds showed good binding modes with higher binding energies. Extension of this work could provide more information towards the optimization of other thieno-pyrmidine derivatives that can be considered as interesting candidates for further development of more potent anticancer agents. The results of this extended work will be reported in due course.

5. Experimental

5.1. Chemistry

5.1.1. General

All Melting points were measured on a Gallen-kamp melting point apparatus and were uncorrected. The IR spectra were recorded on Perkin Elmer 1600 FT IR spectrophotometer using KBr discs (λmax in cm^{-1}). ^{1}H NMR spectra were measured on Bruker spectrometer, TMS was used as internal standard and DMSO-d_6 as solvent, otherwise stated. Chemical shifts (δ) are reported in ppm downfield from TMS and coupling constant (*J*) values were given in Hertz (Hz). Signal multiplicities were represented by s (singlet), d (doublet), t (triplet), q (quadruplet), and m (multiplet). Mass spectra were recorded on a Shimadzu GC-MS-QP 1000X spectrometer operating at 70 e.V. All the new compounds were analyzed for C, H and N and agreed with the proposed structures within ± 0.4% of the theoretical values by the automated CHN analyzer. Reactions progression was monitored by TLC Merck Kieselgel 60 F254 aluminum packed plates. Solvents were purchased from ADWIC Company and used without further purification, hydrazine hydrate (Merck grade), and the other chemicals from Sigma-Aldrich.

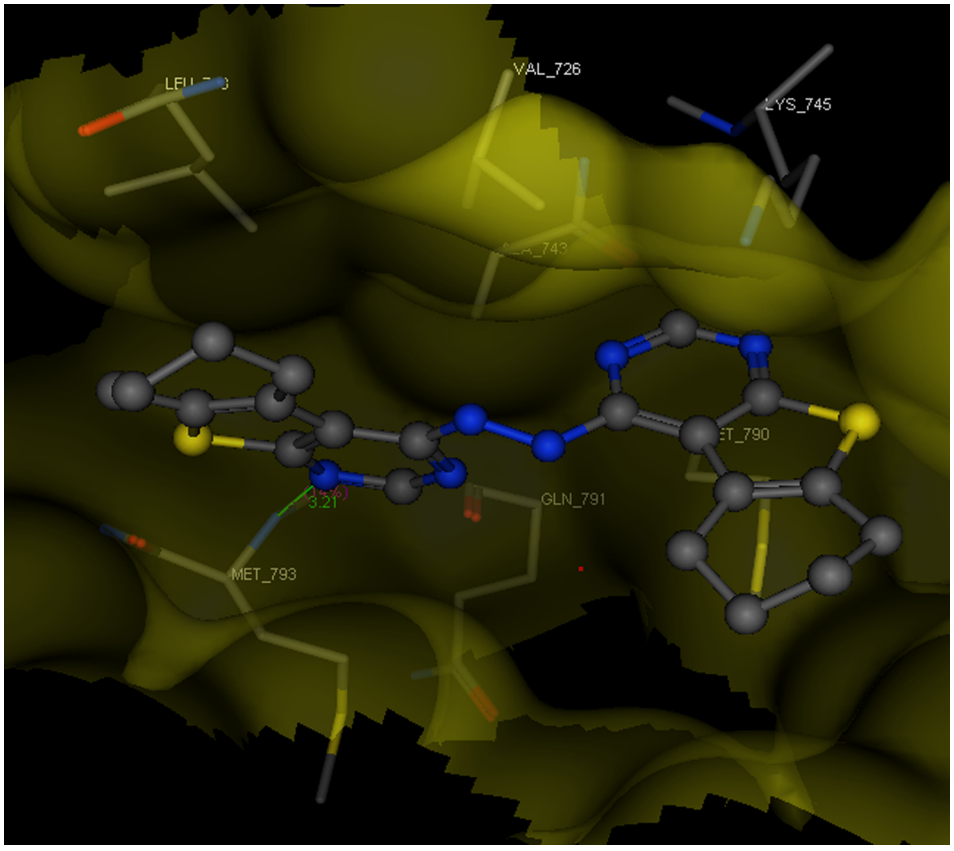

Fig. 14. Calculated binding mode of compound **13k** (grey sticks) within the binding pocket of EGFR^{T790M} receptor. The active pocket has been represented as yellow surface. Important binding sites residues have been depicted as green sticks. (For interpretation of the references to colour in this figure legend, the reader is referred to the web version of this article.)

*5.1.2. 4-chloro-5,6,7,8-tetrahydrobenzo[4,5]thieno[2,3-d]pyrimidine **11***

Step 1: Equimolar amount (0.01 mol) of malononitrile, sulphur and cyclohexanone were taken in a round bottom flask containing 20 ml of ethanol. The mixture was stirred for 5 min then morpholine (0.012 mol) was added dropwise to the reaction mixture at 60 °C with constant stirring over 30 min. Later, the reaction mixture was allowed to stir for 5 h at room temperature and left in refrigerator overnight. The crystals thus formed were collected by filtration and washed with cold ethanol. Further purification by recrystallization from ethanol afford compound **9** in 56% yield, m.p. 145 °C.

Step 2: To a mixture of 2-amino-4,5,6,7-tetrahydrobenzo[*b*]thiophen-carbonitrile (**9**, 0.9 g) and formic acid (10 ml) was added 0.1 ml HCl. After fusion for 3 h, the reaction mixture was cooled and water (20 ml) was added. The precipitated was filtered and washed thoroughly with water and hexanes to give 5,6,7,8 tetrahydrobenzo[4,5]thieno[2,3-*d*]pyrimidin-4(3*H*)-one (**10**, 0.8 g, 77%); m.p. 250 °C; IR: 3520, 2934, 2874, 1660, 1543. ^{1}H NMR (400 MHz, DMSO-d_6) δ 12.27 (br. s., 1H), 7.94 (s, 1H), 2.89 (br. s., 2H), 2.76 (br. s., 2H), 1.76 (br. s., 4H).

Step 3: To a mixture of compound **10** (0.8 g) and $POCl_3$ (10 ml), triethylamine (1 ml) was added dropwise over 30 min. Then, the reaction mixture was heated at 65 °C for 4 h. Water was then added followed by sodium bicarbonate. The resulting mixture was extracted with ethyl acetate. The organic layer was concentrated and the crude compound was crystallized using a mixture of hexanes: ethyl acetate (20:1), to afford 4-chloro-5,6,7,8-tetrahydrobenzo[4,5]thieno[2,3-*d*]pyrimidine (**11**, 0.52 g, 60%); m.p. 118 °C; IR: 2937, 2861, 1660, 1128; ^{1}H NMR (400 MHz, DMSO-d_6) δ 8.72 (s, 1H), 2.96 (br. s., 2H), 2.82 (br. s., 2H), 1.80 (br. s., 4H).

*5.1.3. 4-hydrazinyl-5,6,7,8-tetrahydrobenzo[4,5]thieno[2,3-d]pyrimidine **12***

A solution of absolute ethanol (30 ml) containing pyrimidine **11** (0.5 g, 2.23 mmol) and hydrazine hydrate (0.12 ml, 2.25 mmol) was stirred overnight. The produced solid was filtered and recrystallized from ethanol to give the target compound **12** (95%).

White crystals (95%); m.p. 184–186 (Lit. [66] m.p. 184 °C); IR: 3307, 2939, 2833, 1560; ^{1}H NMR (400 MHz, $CDCl_3$) δ 8.5 (s, 1H), 6.5 (s, 1H), 4.1 (br. s., 2H), 2.8 (t, 4H), 1.98 (m, 4H); ^{13}C NMR (101 MHz, $CDCl_3$) δ 165.1, 158.9, 152.6, 134.1, 125.0, 115.1, 26.3, 25.4, 22.5, 22.4.

*5.1.4. General procedure for preparation of compounds **13a-k***

A mixture of 4-chloro-5,6,7,8-tetrahydrobenzo[4,5]thieno[2,3-*d*]-pyrimidine (**11**, 0.5 g, 2.23 mmol) and appropriate amine (2.23 mmol) was heated under reflux in absolute ethanol for 4 h. After completion, the solid product was filtered off and crystallized from the appropriate solvent to give **13a-k** respectively.

*5.1.4.1. 2-((5,6,7,8-tetrahydrobenzo[4,5]thieno[2,3-d]pyrimidin-4-yl) amino)benzoic acid **13a***. Synthesized according to general procedure 5.1.4 using 2-aminobenzoic acid. The residue was crystallized from Ethanol/DMF to give **13a** (80%) as buff crystals; m.p. 285–287 °C; IR: 3448, 2928, 1689, 1596, 752; ^{1}H NMR (400 MHz, DMSO-d_6) δ 10.98 (s, 1H, OH, exchanged with D_2O), 8.73 (d, J = 9.67 Hz, 1H), 8.49 (s, 1H), 8.01 (dd, J = 1.76, 7.91 Hz, 1H), 7.61 (t, J = 7.03 Hz, 1H), 7.10–7.15 (m, 1H), 3.17 (br. s., 2H), 2.85 (br. s., 2H), 1.87 (br. s., 4H); ESI-MS *m/z*: 297 (M^+ −H,−HCN; 7%), 292 (100%), 280 (72%); Anal. calcd. for $C_{17}H_{15}N_3O_2S$: C, 62.75; H, 4.65; N, 12.91 S, 9.85. Found: C, 62.77; H, 4.63; N, 12.87; S, 9.81.

*5.1.4.2. N-(2-chlorophenyl)-5,6,7,8-tetrahydrobenzo[4,5]thieno[2,3-d] pyrimidin-4-amine **13b***. Synthesized according to general procedure 5.1.4 using 2-chloroaniline. The residue was crystallized from Ethanol/DMF to give **13b** (60%) as white crystals; m.p. 167–170 °C; IR: 3417, 2932, 2855, 1601, 742; ^{1}H NMR (400 MHz, DMSO-d_6) δ 8.34 (s, 1H), 8.11 (br. s., 1H), 7.52 (br. s., 1H), 7.36 (br. s., 1H), 7.19 (br. s., 1H), 3.11 (s, 2H), 2.82 (s, 2H), 1.83 (m, 4H); Anal. calcd. for $C_{16}H_{14}ClN_3S$: C, 60.85; H, 4.47; N, 13.31; S, 10.15. Found: C, 60.90; H, 4.53; N, 13.34; S, 10.19.

*5.1.4.3. N-(4-nitrophenyl)-5,6,7,8-tetrahydrobenzo[4,5]thieno[2,3-d] pyrimidin-4-amine **13c***. Synthesized according to general procedure 5.1.4 using 4-nitrobenzenamine. The residue was crystallized from Ethanol/DMF to give **13c** (77%) as yellow crystals; m.p. 202–204 °C (Lit. [77] m.p. 200 °C); IR: 3435, 3111, 2924, 2862, 853; ^{1}H NMR (400 MHz, DMSO-d_6) δ 8.98 (br. s., 1H), 8.56 (s, 1H), 8.16–8.21 (m, J = 9.23 Hz, 2H), 7.88–7.93 (m, J = 9.23 Hz, 2H), 3.13 (br. s., 2H), 2.82 (br. s., 2H), 1.83 (br. s., 4H); Anal. calcd. for $C_{16}H_{14}N_4O_2S$: C, 58.88; H, 4.32; N, 17.17; S, 9.82. Found: C, 58.84; H, 4.35; N, 17.22; S, 9.85.

*5.1.4.4. N-(4-methoxyphenyl)-5,6,7,8-tetrahydrobenzo[4,5]thieno[2,3-d] pyrimidin-4-amine **13d***. Synthesized according to general procedure 5.1.4 using 4-methoxyaniline. The residue was crystallized from Ethanol to give **13d** (85%) as brown crystals; m.p. 235–237 °C; IR: 3394, 2925, 2858, 1616, 1582, 1247, 832 cm^{-1}; ^{1}H NMR (400 MHz, DMSO-d_6) δ 8.70 (br. s., 1H), 8.45 (s, 1H), 7.45–7.50 (m, J = 8.79 Hz, 2H), 6.95–7.01 (m, J = 8.79 Hz, 2H), 3.78 (s, 3H), 3.13 (br. s., 2H), 2.84 (br. s., 2H), 1.85 (br. s., 4H); ^{13}C NMR (101 MHz, DMSO-d_6) δ 22.2, 22.4, 25.4, 25.7, 55.7, 114.3, 116.8, 126.2, 127.5, 131.1, 134.1, 150.1, 155.4, 157.2, 161.9. Anal. calcd. for $C_{17}H_{17}N_3OS$: C, 65.57; H, 5.50; N, 13.49; S, 10.30. Found: C, 65.59; H, 5.45; N, 13.41; S, 10.1.

*5.1.4.5. 4-((5,6,7,8-tetrahydrobenzo[4,5]thieno[2,3-d]pyrimidin-4-yl) amino)benzoic acid **13e***. Synthesized according to general procedure 5.1.4 using 4-aminobenzoic acid. The residue was crystallized from Ethanol/DMF to give **13e** (88%) as yellow crystals; m.p. 280–282 °C; IR: 3414, 3053, 2930, 1803, 1655; ^{1}H NMR (400 MHz, DMSO-d_6) δ 8.58 (s, 1H), 8.52 (s, 1H), 7.90–7.94 (m, J = 8.79 Hz, 2H), 7.79–7.82 (m, J = 8.79 Hz, 2H), 3.15 (br. s., 2H), 2.85 (br. s., 2H), 1.85 (br. s., 4H); ESI-MS *m/z*: 325 (M^+, 98%), 53.56 (100%); Anal. calcd. for $C_{17}H_{15}N_3O_2S$: C, 62.75; H, 4.65; N 12.9; S, 9.85. Found: C, 62.72; H, 4.70; N; 12.95; S, 9.82

*5.1.4.6. 1-(4-((5,6,7,8-tetrahydrobenzo[4,5]thieno[2,3-d]pyrimidin-4-yl) amino)phenyl)ethan-1-one **13f***. Synthesized according to general procedure 5.1.4 using 4-aminoacetophenone. The residue was crystallized from Ethanol to give **13f** (67%) as brown crystals; m.p. 181–183 °C; IR: 3457, 3051, 2925, 2859, 1666, 1600, 811 cm^{-1}; ^{1}H NMR (400 MHz, DMSO-d_6) δ 8.49 (s, 1H), 7.92–7.96 (m, J = 9.23 Hz, 2H), 7.80–7.84 (m, J = 8.79 Hz, 2H), 3.14 (br. s., 2H), 2.84 (br. s., 2H), 2.54 (s, 3H), 1.85 (br. s., 4H); ESI-MS *m/z*: 323 (M^+, 100%), 308 (23%), 80 (27%), 69 (88%); Anal. calcd. for $C_{18}H_{17}N_3OS$: C, 66.85; H, 5.30; N, 12.99; S, 9.91. Found: C, 66.86; H, 5.34; N, 12.96; S, 9.87.

*5.1.4.7. 5-iodo-2-((5,6,7,8-tetrahydrobenzo[4,5]thieno[2,3-d]pyrimidin-4-yl)amino)benzoic acid **13g***. Synthesized according to general procedure 5.1.4 using 2-amino-5-iodobenzoic acid. The residue was crystallized from DMF to give **13g** (80%) as buff crystals; m.p. 250–252 °C; IR: 3211, 3155, 3075, 2925, 2853, 1693, 1587, 579; ^{1}H NMR (400 MHz, DMSO-d_6) δ 10.92 (s, 1H), 8.59 (d, J = 8.79 Hz, 1H), 8.49 (s, 1H), 8.22 (d, J = 2.20 Hz, 1H), 7.89 (dd, J = 2.20, 9.23 Hz, 1H), 3.12 (br. s., 2H), 2.84 (br. s., 2H), 1.85 (br. s., 4H); ESI-MS *m/z*: 451 (M^+, 10%), 433 (100%); Anal. calcd. for $C_{17}H_{14}IN_3O_2S$: C, 45.24; H, 3.13; N, 9.31; S, 7.11. Found: C, 45.23; H, 3.15; N, 9.33; S, 7.13.

*5.1.4.8. 4-((5,6,7,8-tetrahydrobenzo[4,5]thieno[2,3-d]pyrimidin-4-yl) amino)phenol **13h***. Synthesized according to general procedure 5.1.4 using 4-aminophenol. The residue was crystallized from Ethanol/DMF to give **13h** (80%) as brown crystals; m.p. 230–333 °C; IR: 3409, 3201, 2948, 2853, 1619, 1585. 1220 cm^{-1}; ^{1}H NMR (400 MHz, DMSO-d_6) δ 8.88 (br. s., 1H), 8.46 (s, 1H), 7.28–7.36 (m, J = 8.79 Hz, 2H),

6.79–6.88 (m, J = 8.79 Hz, 2H), 3.11 (br. s., 2H), 2.84 (br. s., 2H), 1.84 (br. s., 4H); ^{13}C NMR (101 MHz, DMSO-d_6) δ 162.2, 155.0, 150.0, 148.0, 133.3, 129.1, 127.1, 125.9, 116.2, 115.2, 25.4, 25.0, 22.0, 21.9; Anal. calcd. for $C_{16}H_{15}N_3OS$: C, 64.62; H, 5.08; N, 14.13; S, 10.87. Found: C, 64.66; H, 5.10; N, 14.15; S, 10.83.

5.1.4.9. 2-((5,6,7,8-tetrahydrobenzo[4,5]thieno[2,3-d]pyrimidin-4-yl) amino)-4,5,6,7-tetrahydrobenzo[b]thiophene-3-carbonitrile ***13i***. Synthesized according to general procedure 5.1.4 using 2-amino-4,5,6,7-tetrahydrobenzo[*b*]thiophene-3-carbonitrile. The residue was crystallized from Ethanol/DMF to give **13i** (90%) as yellow crystals; m.p. 220–222 °C; IR: 3435, 2928, 2850, 2233, 1628, 1586, 1502; ^{1}H NMR (400 MHz, DMSO-d_6) δ 9.26 (s, 1H), 2.99 (br. s., 2H), 2.93 (br. s., 2H), 2.90 (br. s., 2H), 2.78 (br. s., 2H), 1.87 (br. s., 4H), 1.79 (br. s., 4H); ESI-MS *m/z*: 367 (M^{+1}, 6.9%), 72 (81%), 44 (100%); Anal. calcd. for $C_{19}H_{18}N_4S_2$: C, 62.27; H, 4.95; N, 15.29; S, 17.50. Found: C, 62.30; H, 5.99; N, 15.30; S, 17.42.

5.1.4.10. N1,N2-bis(5,6,7,8-tetrahydrobenzo[4,5]thieno[2,3-d]pyrimidin-4-yl)benzene-1,2-diamine ***13j***. Synthesized according to general procedure 5.1.4 using 2-benzene-1,2-diamine. The residue was washed with hot DMSO to give **13j** (85%) as white crystal; m.p. 269–271 °C; IR: 3370, 3318, 3122, 2928, 2908, 1648, 1570; ^{1}H NMR (400 MHz, DMSO-d_6) δ 8.17 (s, 2H), 6.77 (br. s., 4H), 2.90 (br. s., 4H), 2.74 (br. s., 4H), 1.80 (br. s., 8H); ESI-MS *m/z*: 484 (M^+, 5.68%), 323 (100%), 279 (54.0%); Anal. calcd. for $C_{26}H_{24}N_6S_2$: C, 64.44; H, 4.99; N, 17.34; S, 13.23. Found: C, 64.45; H, 5.08; N, 17.37; S, 13.22.

5.1.4.11. 1,2-bis(5,6,7,8-tetrahydrobenzo[4,5]thieno[2,3-d]pyrimidin-4-yl) hydrazine ***13k***. Synthesized according to general procedure 5.1.4 using 4-hydrazinyl-5,6,7,8-tetrahydrobenzo[4,5]thieno[2,3-*d*]pyrimidine (**12**). The residue was crystallized from Ethanol/DMF to give **13k** (90%) as grey powder; m.p. > 300 °C, IR: 3238, 2929, 2835, 1621, 1582; ESI-MS *m/z*: 409 (M^{+1}, 2.03%), 408 (M^+, 1.7%), 303 (33%), 264 (67%), 77 (100%). Anal. calcd. for $C_{20}H_{20}N_6S_2$: C, 58.80; H, 4.93; N, 20.57. Found: C, 58.85; H, 4.97; N, 20.60.

Alternative method for preparation of ***13k:*** A mixture of compound **11** (0.5 g, 2.23 mmol) and half equivalent of hydrazine hydrate (0.060 ml, 1.30 mmol) was refluxed for 4 h in absolute ethanol (30 ml). The formed solid product was filtered off and washed with hot DMSO to give **13k**.

5.1.5. General procedure for preparation of compounds ***14–16***

A mixture of 4-chloro-5,6,7,8-tetrahydrobenzo[4,5]thieno[2,3-*d*]-pyrimidine **11** (0.5 g, 2.23 mmol) and (2.3 mmol) each of sodium azide (0.15 g), thiosemicarbazide hydrochloride (0.28 g) or *N*-phenylthiourea (0.34gm) was refluxed for 4 h in glacial acetic acid (15 ml). After cooling, the mixture was poured over ice/water mixture. The formed solid was filtered, dried and crystallized from (Ethanol/DMF) to give the target compounds **14**, **15** and **16**, respectively.

5.1.5.1. 8,9,10,11-tetrahydrobenzo[4,5]thieno[3,2-e]tetrazolo[1,5-c] pyrimidine ***14***. Yield: 70%; creamy crystals; m.p. 130 °C (Lit. [66] m.p. 132 °C). ^{1}H NMR (400 MHz, $CDCl_3$) δ 9.42 (s, 1H), 3.12 (br. s., 2H), 3.25 (br. s., 2H), 2.09 (br. s., 4H).

5.1.5.2. 8,9,10,11-tetrahydrobenzo[4,5]thieno[3,2-e][1,2,4]triazolo[4,3-c]pyrimidine-3(2H)-thione ***15***. Yield: 60%; brown crystals; m.p. 272 °C (Lit. [66] m.p. 275–277 °C); ^{1}H NMR (400 MHz, DMSO-d_6) δ 9.42 (s, 1H), 2.99 (br. s., 1H), 2.91 (br. s., 2H), 2.79 (br. s., 1H), 1.87 (br. s., 2H), 1.80 (br. s., 2H).

5.1.5.3. 5,6,7,8-tetrahydrobenzo[4,5]thieno[2,3-d]pyrimidine-4-thiol ***16***. Yield: 65%; white crystals; m.p. 243 °C (Lit. [66] m.p. 241–243 °C). ^{1}H NMR (400 MHz, DMSO-d_6) δ 13.68 (br. s., 1H), 8.08 (d, J = 3.52 Hz, 1H), 3.17 (br. s., 2H), 2.76 (br. s., 2H), 1.77 (d, J = 5.71 Hz, 4H).

5.2. Biological evaluation

5.2.1. $EGFR^{WT}$ and HER2 kinase inhibitory assay

The *in vitro* inhibitory activities of the synthesized compounds against $EGFR^{WT}$ and HER2 were carried out using EGFR and HER2 Kinase Assay Kit (BPS biosciences). At first, $EGFR^{WT}$/HER2 and their substrates were incubated with the synthesized compounds in enzymatic buffer for 40 min at 30 °C in order to start the enzymatic reaction. The reaction was stopped by addition of detection reagent (Kinase-Glo Max reagent), followed by incubation at room temperature for 15 min. Then the IC_{50} values were determined by ROBONIK P2000 ELISA reader. All samples and controls were tested in duplicate.

5.2.2. $EGFR^{T790M}$ kinase inhibitory assay

The *in vitro* inhibitory activities of the synthesized compounds against $EGFR^{T790M}$ were carried out using $EGFR^{T790M}$/ADP-Glo™ Kinase Assay system (Promega). At first, $EGFR^{T790M}$ and their substrates were incubated with the synthesized compounds in enzymatic buffer for 60 min at room temperature in order to start the enzymatic reaction. The reaction was stopped by addition of detection reagent (ADP-Glo™ reagent), followed by incubation at room temperature for 40 min. Then, kinase detection reagent was added, and the mixture was incubated for further 30 min. The IC_{50} values were determined after luminescence record. All samples and controls were tested in duplicate.

5.2.3. In vitro anti-proliferative activities

Anti-proliferative activities of the synthesized compounds were carried out based on MTT assay [68]. The kit was used according to manufacturer's protocol. Briefly, HepG2, HCT-116, MCF-7 and A431 cell lines were seeded at a density of 6000 cells/well in quadruplicates wells of a 96-well tissue culture plates with 50 µl of complete media. Cells were allowed to attach and grow overnight at 37 °C in a 5% CO_2 humidified atmosphere. Then, for each well, the growth medium was exchanged with 0.1 ml of fresh medium containing graded concentrations of the test compounds to be or equal DMSO and incubated for two days. Then 10 µl MTT solution (5 µg/ml) was added to each well, and the cells were incubated for additional 4 h. The crystals of MTT-formazan were dissolved in 100 µl of DMSO; the absorbance of each well was measured at 490 nm using an automatic ELISA reader system (TECAN, CHE). The IC_{50} values were calculated using the nonlinear regression fitting models (Graph Pad, Prism Version 5). The means of three independent experiments gave the reported results. Statistical differences were analyzed according to one-way ANOVA test wherein the differences were considered to be significant at $p < 0.05$.

5.2.4. In-vitro DNA-Flow cytometric (cell cycle) analysis

To determine the distribution of cell lines in each phase of cell cycle, the PI was used to stain the DNA content of each cell line. At a density of 1×10^6–3×10^6 cells/dish, MCF-7 cells were seeded in 30 mm tissue culture plates in 5 ml of complete medium. Cells were incubated and allowed to adhere in CO_2 atmosphere. After 24 h adherence, cells were incubated with compound **13k** for 24 h. Then, the cell pellets were collected by trypsinization and washed twice with PBS washing buffer and fixed with 70% ice cold ethanol for a minimum of 24 h at −20 °C. The cells were stained with PI and RNase Staining Solution according to the manufacturer's instructions. Cell-cycle distribution was evaluated using a BD FACSCalibur flow cytometer. Data were collected from three individual experiments.

5.2.5. Annexin V-FITC apoptosis assay

Annexin V-FITC apoptosis detection kit (BD biosciences) was used to quantify the percentage of cells undergoing apoptosis and to determine the mode of cell death whether by apoptosis or necrosis in the presence or absence of the active compound **13k**. The experiment was carried out according to the manufacturer's protocol. Briefly, cells were seeded (1×10^6–3×10^6) per dish and allowed to adhere overnight in CO_2

incubator. Following 24 h incubation, Compound **13k** was added, and plates were incubated for another 24 h in CO_2 atmosphere. Both adherent and nonadherent cells were trypsinized, collected and centrifuged for 5 min at 300g. Cell pellets were washed with 2 ml of cold PBS twice, re-suspended in 100 µl of 1X binding buffer and stained with 5 µl of FITC Annexin V and 5 µl of PI for 15 min in the dark at room temperature. Following incubation, 1 ml of 1X binding buffer was added and the analysis was done using flow cytometer within an hour. Data was collected from three individual Experiments.

5.3. Molecular modeling

Crystallographic structures of $EGFR^{WT}$ and $EGFR^{T790M}$ were retrieved from Protein Data Bank [http://www.rscb.org./pdb; code: 4HJO, resolution 2.75 Å; code: 3W2O, resolution 2.35 Å, respectively] and considered as target for docking simulation. The docking analysis was performed using MOE software to evaluate the free energies and binding mode of the designed molecules against $EGFR^{WT}$ and $EGFR^{T790M}$. At first, the protein structures were protonated, and the hydrogen atoms were hided. Then, the energy was minimized, and the binding pockets of the protein were defined.

The 2D structures of the synthesized compounds and erlotinib were sketched using ChemBioDraw Ultra 14.0 and saved as MOL format. Then, the saved files were opened using MOE and 3D structures were protonated. Next, energy minimization was applied. Before docking the synthesized compounds, validation of the docking protocol was carried out by running the simulation only using the co-crystallized ligands and low RMSD between docked and crystal conformations. The molecular docking of the synthesized compounds and the co-crystallized ligand was performed using a default protocol. In each case, 30 docked structures were generated using genetic algorithm searches.

Funding

This research did not receive any specific grant from funding agencies in the public, commercial, or not-for-profit sectors.

Acknowledgement

Authors are thankful to the biologists of VACSERA CO., Giza, Egypt for providing laboratory facilities for biological testing.

Appendix A. Supplementary material

Spectral data (^1H, ^{13}C NMR, IR, and ESI-MS) are available in a separated file. Supplementary data to this article can be found online at https://doi.org/10.1016/j.bioorg.2019.102944. These data include MOL files and InChiKeys of the most important compounds described in this article.

References

[1] World Health Organization: Cancer – Key Facts, 2018. < http://www.who.int/news-room/fact-sheets/detail/cancer > .
[2] N. Parsa, Environmental factors inducing human cancers, Iran. J. Publ. Health 41 (2012) 1–9.
[3] P. Blume-Jensen, T. Hunter, Oncogenic kinase signalling, Nature 411 (2001) 355–365.
[4] D. Fabbro, S.W. Cowan-Jacob, H. Moebitz, Ten things you should know about protein kinases: IUPHAR Review 14, Br. J. Pharmacol. 172 (2015) 2675–2700.
[5] M. Huang, A. Shen, J. Ding, M. Geng, Molecularly targeted cancer therapy: some lessons from the past decade, Trends Pharmacol. Sci. 35 (2014) 41–50.
[6] W.M. Eldehna, M.F. Abo-Ashour, A. Nocentini, P. Gratteri, I.H. Eissa, M. Fares, O.E. Ismael, H.A. Ghabbour, M.M. Elaasser, H.A. Abdel-Aziz, C.T. Supuran, Novel 4/3-((4-oxo-5-(2-oxoindolin-3-ylidene)thiazolidin-2-ylidene)amino) benzenesulfonamides: synthesis, carbonic anhydrase inhibitory activity, anticancer activity and molecular modelling studies, Eur. J. Med. Chem. 139 (2017) 250–262.
[7] M.K. Ibrahim, M.S. Taghour, A.M. Metwaly, A. Belal, A.B.M. Mehany, M.A. Elhendawy, M.M. Radwan, A.M. Yassin, N.M. El-Deeb, E.E. Hafez, M.A. ElSohly, I.H. Eissa, Design, synthesis, molecular modeling and antiproliferative evaluation of novel quinoxaline derivatives as potential DNA intercalators and topoisomerase II inhibitors, Eur. J. Med. Chem. 155 (2018) 117–134.
[8] F. Muth, M. Günther, S.M. Bauer, E. Döring, S. Fischer, J. Maier, P. Drückes, J. Köppler, J. Trappe, U. Rothbauer, P. Koch, S.A. Laufer, Tetra-substituted pyridinylimidazoles as dual inhibitors of p38α mitogen-activated protein kinase and c-Jun N-terminal kinase 3 for potential treatment of neurodegenerative diseases, J. Med. Chem. 58 (2015) 443–456.
[9] J.D. Clark, M.E. Flanagan, J.-B. Telliez, Discovery and development of Janus Kinase (JAK) inhibitors for inflammatory diseases, J. Med. Chem. 57 (2014) 5023–5038.
[10] A.S. Banks, F.E. McAllister, J.P.G. Camporez, P.-J.H. Zushin, M.J. Jurczak, D. Laznik-Bogoslavski, G.I. Shulman, S.P. Gygi, B.M. Spiegelman, An ERK/Cdk5 axis controls the diabetogenic actions of PPARγ, Nature 517 (2014) 391.
[11] R. Kikuchi, K. Nakamura, S. MacLauchlan, D.T.-M. Ngo, I. Shimizu, J.J. Fuster, Y. Katanasaka, S. Yoshida, Y. Qiu, T.P. Yamaguchi, T. Matsushita, T. Murohara, N. Gokce, D.O. Bates, N.M. Hamburg, K. Walsh, An antiangiogenic isoform of VEGF-A contributes to impaired vascularization in peripheral artery disease, Nat. Med. 20 (2014) 1464.
[12] M.A. Olayioye, R.M. Neve, H.A. Lane, N.E. Hynes, The ErbB signaling network: receptor heterodimerization in development and cancer, EMBO J. 19 (2000) 3159.
[13] M.L.D.C. Barbosa, L.M. Lima, R. Tesch, C.M.R. Sant'Anna, F. Totzke, M.H.G. Kubbutat, C. Schächtele, S.A. Laufer, E.J. Barreiro, Novel 2-chloro-4-anilino-quinazoline derivatives as EGFR and VEGFR-2 dual inhibitors, Eur. J. Med. Chem. 71 (2014) 1–14.
[14] Y. Chen, J. Wu, A. Wang, Z. Qi, T. Jiang, C. Chen, F. Zou, C. Hu, W. Wang, H. Wu, Z. Hu, W. Wang, B. Wang, L. Wang, T. Ren, S. Zhang, Q. Liu, J. Liu, Discovery of N-(5-((5-chloro-4-((2-(isopropylsulfonyl)phenyl)amino)pyrimidin-2-yl)amino)-4-methoxy-2-(4-methyl-1,4-diazepan-1-yl)phenyl)acrylamide (CHMFL-ALK/EGFR-050) as a potent ALK/EGFR dual kinase inhibitor capable of overcoming a variety of ALK/EGFR associated drug resistant mutants in NSCLC, Eur. J. Med. Chem. 139 (2017) 674–697.
[15] Y.A.M.M. Elshaier, M.A. Shaaban, M.K. Abd El Hamid, M.H. Abdelrahman, M.A. Abou-Salim, S.M. Elgazwi, F. Halaweish, Design and synthesis of pyrazolo[3,4-d]pyrimidines: nitric oxide releasing compounds targeting hepatocellular carcinoma, Bioorg. Med. Chem. 25 (2017) 2956–2970.
[16] J. Chang, H. Ren, M. Zhao, Y. Chong, W. Zhao, Y. He, Y. Zhao, H. Zhang, C. Qi, Development of a series of novel 4-anlinoquinazoline derivatives possessing quinazoline skeleton: design, synthesis, EGFR kinase inhibitory efficacy, and evaluation of anticancer activities in vitro, Eur. J. Med. Chem. 138 (2017) 669–688.
[17] A.A. Gaber, A.H. Bayoumi, A.M. El-morsy, F.F. Sherbiny, A.B.M. Mehany, I.H. Eissa, Design, synthesis and anticancer evaluation of 1H-pyrazolo[3,4-d]pyrimidine derivatives as potent EGFRWT and EGFRT790M inhibitors and apoptosis inducers, Bioorg. Chem. 80 (2018) 375–395.
[18] I.H. Eissa, A.M. El-Naggar, M.A. El-Hashash, Design, synthesis, molecular modeling and biological evaluation of novel 1H-pyrazolo[3,4-b]pyridine derivatives as potential anticancer agents, Bioorg. Chem. 67 (2016) 43–56.
[19] A.M. El-Naggar, M.M. Abou-El-Regal, S.A. El-Metwally, F.F. Sherbiny, I.H.J.M.D. Eissa, Synthesis, characterization and molecular docking studies of thiouracil derivatives as potent thymidylate synthase inhibitors and potential anticancer agents 21 (2017) 967–983.
[20] H.E. Ibrahim, M.E.-N. Abeer, E.A.A.E.-S. Nour, S.A.Y. Ahmed, Design and discovery of novel quinoxaline derivatives as dual DNA intercalators and topoisomerase II inhibitors, Anti-Cancer Agents Med. Chem. 18 (2018) 195–209.
[21] N. Iqbal, N. Iqbal, Human epidermal growth factor receptor 2 (HER2) in cancers: overexpression and therapeutic implications %J, Mol. Biol. Int. (2014) 9.
[22] J.L. Hsu, M.-C. Hung, The role of HER2, EGFR, and other receptor tyrosine kinases in breast cancer, Cancer Metast. Rev. 35 (2016) 575–588.
[23] L.A. Elferink, V.A. Resto, Receptor-tyrosine-kinase-targeted therapies for head and neck cancer, J. Signal Trans. 2011 (2011) 982879.
[24] B. Markman, F. Javier Ramos, J. Capdevila, J. Tabernero, EGFR and KRAS in colorectal cancer, Adv. Clin. Chem. 51 (2010) 71–119.
[25] M. Brevet, M. Arcila, M. Ladanyi, Assessment of EGFR mutation status in lung adenocarcinoma by immunohistochemistry using antibodies specific to the two major forms of mutant EGFR, J. Mol. Diagn.: JMD 12 (2010) 169–176.
[26] E. Padfield, H.P. Ellis, K.M. Kurian, Current therapeutic advances targeting EGFR and EGFRvIII in glioblastoma, Front. Oncol. 5 (2015) 5.
[27] P.M. Harari, Epidermal growth factor receptor inhibition strategies in oncology, Endocr. Relat. Cancer 11 (2004) 689–708.
[28] P. Bonomi, Erlotinib: a new therapeutic approach for non-small cell lung cancer, Expert Opin. Invest. Drugs 12 (2003) 1395–1401.
[29] J.F. Vansteenkiste, Gefitinib (Iressa®): a novel treatment for non-small cell lung cancer, Expert Rev. Anticancer Ther. 4 (2004) 5–17.
[30] G.R. Oxnard, M.E. Arcila, C.S. Sima, G.J. Riely, J. Chmielecki, M.G. Kris, W. Pao, M. Ladanyi, V.A. Miller, Acquired resistance to EGFR tyrosine kinase inhibitors in EGFR-mutant lung cancer: distinct natural history of patients with tumors harboring the T790M mutation, Clin. Cancer Res.: Off. J. Am. Assoc. Cancer Res. 17 (2011) 1616–1622.
[31] S.-H.I. Ou, Second-generation irreversible epidermal growth factor receptor (EGFR) tyrosine kinase inhibitors (TKIs): a better mousetrap? A review of the clinical evidence, Crit. Rev. Oncol./Hematol. 83 (2012) 407–421.
[32] J.A. McIntyre, J. Castaner, P.A. Leeson, Canertinib dihydrochloride, Drugs Fut. 30 (8) (2005) 771.
[33] D. Li, L. Ambrogio, T. Shimamura, S. Kubo, M. Takahashi, L.R. Chirieac, R.F. Padera, G.I. Shapiro, A. Baum, F. Himmelsbach, W.J. Rettig, M. Meyerson, F. Solca, H. Greulich, K.K. Wong, BIBW2992, an irreversible EGFR/HER2 inhibitor highly effective in preclinical lung cancer models, Oncogene 27 (2008) 4702–4711.
[34] G. Giaccone, Y. Wang, Strategies for overcoming resistance to EGFR family tyrosine

kinase inhibitors, Cancer Treat. Rev. 37 (2011) 456–464.
[35] V.A. Miller, V. Hirsh, J. Cadranel, Y.M. Chen, K. Park, S.W. Kim, C. Zhou, W.C. Su, M. Wang, Y. Sun, D.S. Heo, L. Crino, E.H. Tan, T.Y. Chao, M. Shahidi, X.J. Cong, R.M. Lorence, J.C. Yang, Afatinib versus placebo for patients with advanced, metastatic non-small-cell lung cancer after failure of erlotinib, gefitinib, or both, and one or two lines of chemotherapy (LUX-Lung 1): a phase 2b/3 randomised trial, Lancet Oncol. 13 (2012) 528–538.
[36] S.S. Ramalingam, P.A. Jänne, T. Mok, K. O'Byrne, M.J. Boyer, J. Von Pawel, A. Pluzanski, M. Shtivelband, L.I. Docampo, J. Bennouna, H. Zhang, J.Q. Liang, J.P. Doherty, I. Taylor, C.B. Mather, Z. Goldberg, J. O'Connell, L. Paz-Ares, Dacomitinib versus erlotinib in patients with advanced-stage, previously treated non-small-cell lung cancer (ARCHER 1009): a randomised, double-blind, phase 3 trial, Lancet Oncol. 15 (2014) 1369–1378.
[37] A.O. Walter, R.T. Sjin, H.J. Haringsma, K. Ohashi, J. Sun, K. Lee, A. Dubrovskiy, M. Labenski, Z. Zhu, Z. Wang, M. Sheets, T. St Martin, R. Karp, D. van Kalken, P. Chaturvedi, D. Niu, M. Nacht, R.C. Petter, W. Westlin, K. Lin, S. Jaw-Tsai, M. Raponi, T. Van Dyke, J. Etter, Z. Weaver, W. Pao, J. Singh, A.D. Simmons, T.C. Harding, A. Allen, Discovery of a mutant-selective covalent inhibitor of EGFR that overcomes T790M-mediated resistance in NSCLC, Cancer Disc. 3 (2013) 1404–1415.
[38] D.A. Cross, S.E. Ashton, S. Ghiorghiu, C. Eberlein, C.A. Nebhan, P.J. Spitzler, J.P. Orme, M.R. Finlay, R.A. Ward, M.J. Mellor, G. Hughes, A. Rahi, V.N. Jacobs, M. Red Brewer, E. Ichihara, J. Sun, H. Jin, P. Ballard, K. Al-Kadhimi, R. Rowlinson, T. Klinowska, G.H. Richmond, M. Cantarini, D.W. Kim, M.R. Ranson, W. Pao, AZD9291, an irreversible EGFR TKI, overcomes T790M-mediated resistance to EGFR inhibitors in lung cancer, Cancer Disc. 4 (2014) 1046–1061.
[39] W. Zhou, D. Ercan, L. Chen, C.H. Yun, D. Li, M. Capelletti, A.B. Cortot, L. Chirieac, R.E. Iacob, R. Padera, J.R. Engen, K.K. Wong, M.J. Eck, N.S. Gray, P.A. Janne, Novel mutant-selective EGFR kinase inhibitors against EGFR T790M, Nature 462 (2009) 1070–1074.
[40] P.A. Jänne, J.C.-H. Yang, D.-W. Kim, D. Planchard, Y. Ohe, S.S. Ramalingam, M.-J. Ahn, S.-W. Kim, W.-C. Su, L. Horn, D. Haggstrom, E. Felip, J.-H. Kim, P. Frewer, M. Cantarini, K.H. Brown, P.A. Dickinson, S. Ghiorghiu, M. Ranson, AZD9291 in EGFR inhibitor-resistant non–small-cell, Lung Cancer 372 (2015) 1689–1699.
[41] L.V. Sequist, J.-C. Soria, J.W. Goldman, H.A. Wakelee, S.M. Gadgeel, A. Varga, V. Papadimitrakopoulou, B.J. Solomon, G.R. Oxnard, R. Dziadziuszko, D.L. Aisner, R.C. Doebele, C. Galasso, E.B. Garon, R.S. Heist, J. Logan, J.W. Neal, M.A. Mendenhall, S. Nichols, Z. Piotrowska, A.J. Wozniak, M. Raponi, C.A. Karlovich, S. Jaw-Tsai, J. Isaacson, D. Despain, S.L. Matheny, L. Rolfe, A.R. Allen, D.R. Camidge, Rociletinib in EGFR-mutated non–small-cell, Lung Cancer 372 (2015) 1700–1709.
[42] Z.H. Tang, J.J. Lu, Osimertinib resistance in non-small cell lung cancer: mechanisms and therapeutic strategies, Cancer Lett. 420 (2018) 242–246.
[43] C.A. Eberlein, D. Stetson, A.A. Markovets, K.J. Al-Kadhimi, Z. Lai, P.R. Fisher, C.B. Meador, P. Spitzler, E. Ichihara, S.J. Ross, M.J. Ahdesmaki, A. Ahmed, L.E. Ratcliffe, E.L. O'Brien, C.H. Barnes, H. Brown, P.D. Smith, J.R. Dry, G. Beran, K.S. Thress, B. Dougherty, W. Pao, D.A. Cross, Acquired resistance to the mutant-selective EGFR inhibitor AZD9291 is associated with increased dependence on RAS signaling in preclinical models, Cancer Res. 75 (2015) 2489–2500.
[44] E.Z. Elrazaz, R.A.T. Serya, N.S.M. Ismail, D.A. Abou El Ella, K.A.M. Abouzid, Thieno [2,3-d]pyrimidine based derivatives as kinase inhibitors and anticancer agents, Future J. Pharm. Sci. 1 (2015) 33–41.
[45] M.E. Adly, E.M. Gedawy, A.A. El-Malah, F.A. El-Telbany, Synthesis of novel thieno [2,3-d]pyrimidine derivatives and evaluation of their cytotoxicity and EGFR inhibitory activity, Anti-Cancer Agents Med. Chem. 18 (2018) 747–756.
[46] X. Ji, T. Peng, X. Zhang, J. Li, W. Yang, L. Tong, R. Qu, H. Jiang, J. Ding, H. Xie, H. Liu, Design, synthesis and biological evaluation of novel 6-alkenylamides substituted of 4-anilinothieno[2,3-d]pyrimidines as irreversible epidermal growth factor receptor inhibitors, Bioorg. Med. Chem. 22 (2014) 2366–2378.
[47] Y. Deng, X. Zhou, S. Kugel Desmoulin, J. Wu, C. Cherian, Z. Hou, L.H. Matherly, A. Gangjee, Synthesis and biological activity of a novel series of 6-substituted thieno [2,3-d]pyrimidine antifolate inhibitors of purine biosynthesis with selectivity for high affinity folate receptors over the reduced folate carrier and proton-coupled folate transporter for cellular entry, J. Med. Chem. 52 (2009) 2940–2951.
[48] C.R. Yang, B. Peng, S.L. Cao, T.T. Ren, W. Jiang, F.C. Wang, Y.S. Li, G. Wang, Z. Li, S. Xu, J. Liao, H. Wang, J. Li, X. Xu, Synthesis, cytotoxic evaluation and target identification of thieno[2,3-d]pyrimidine derivatives with a dithiocarbamate side chain at C2 position, Eur. J. Med. Chem. 154 (2018) 324–340.
[49] C. Tian, Z. Han, Y. Li, M. Wang, J. Yang, X. Wang, Z. Zhang, J. Liu, Synthesis and biological evaluation of 2,6-disubstituted-9H-purine, 2,4-disubstitued-thieno[3,2-d] pyrimidine and -7H-pyrrolo[2,3-d]pyrimidine analogues as novel CHK1 inhibitors, Eur. J. Med. Chem. 151 (2018) 836–848.
[50] C. Oh, H. Kim, J.S. Kang, J. Yun, J. Sim, H.M. Kim, G. Han, Synthetic strategy for increasing solubility of potential FLT3 inhibitor thieno[2,3-d]pyrimidine derivatives through structural modifications at the C2 and C6 positions, Bioorg. Med. Chem. Lett. 27 (2017) 496–500.
[51] K. Niefind, N. Bischoff, A.G. Golub, V.G. Bdzhola, A.O. Balanda, A.O. Prykhod'ko, S.M. Yarmoluk, Structural hypervariability of the two human protein kinase CK2 catalytic subunit paralogs revealed by complex structures with a flavonol- and a thieno[2,3-d]pyrimidine-based inhibitor, Pharmaceuticals (Basel) 10 (2017).
[52] J. Li, W. Gu, X. Bi, H. Li, C. Liao, C. Liu, W. Huang, H. Qian, Design, synthesis, and biological evaluation of thieno[2,3-d]pyrimidine derivatives as novel dual c-Met and VEGFR-2 kinase inhibitors, Bioorg. Med. Chem. 25 (2017) 6674–6679.
[53] R.K. Gill, V. Kumar, M. Bishnoi, K. Yadav, K.K. Kondepudi, J. Bariwal, Design and green synthesis of thieno[2,3-d]pyrimidine analogues as potential antiproliferative agents, Anti-Cancer Agents Med. Chem. 17 (2017) 701–711.
[54] J. Yong, C. Lu, X. Wu, Synthesis of isoxazole moiety containing thieno[2,3-d]pyrimidine derivatives and preliminarily in vitro anticancer activity (Part II), Anti-Cancer Agents Med. Chem. 15 (2015) 1148–1155.
[55] M.M. Kandeel, H.M. Refaat, A.E. Kassab, I.G. Shahin, T.M. Abdelghany, Synthesis, anticancer activity and effects on cell cycle profile and apoptosis of novel thieno [2,3-d]pyrimidine and thieno[3,2-e] triazolo[4,3-c]pyrimidine derivatives, Eur. J. Med. Chem. 90 (2015) 620–632.
[56] J.S. Yang, C.H. Park, C. Lee, H. Kim, C. Oh, Y. Choi, J.S. Kang, J. Yun, J.H. Jeong, M.H. Kim, G. Han, Synthesis and biological evaluation of novel thieno[2,3-d]pyrimidine-based FLT3 inhibitors as anti-leukemic agents, Eur. J. Med. Chem. 85 (2014) 399–407.
[57] S. Kjaer, M. Linch, A. Purkiss, B. Kostelecky, P.P. Knowles, C. Rosse, P. Riou, C. Soudy, S. Kaye, B. Patel, E. Soriano, J. Murray-Rust, C. Barton, C. Dillon, J. Roffey, P.J. Parker, N.Q. McDonald, Adenosine-binding motif mimicry and cellular effects of a thieno[2,3-d]pyrimidine-based chemical inhibitor of atypical protein kinase C isoenzymes, Biochem. J. 451 (2013) 329–342.
[58] S.E. Abbas, N.M. Abdel Gawad, R.F. George, Y.A. Akar, Synthesis, antitumor and antibacterial activities of some novel tetrahydrobenzo[4,5]thieno[2,3-d]pyrimidine derivatives, Eur. J. Med. Chem. 65 (2013) 195–204.
[59] S.N. Milik, A.K. Abdel-Aziz, D.S. Lasheen, R.A.T. Serya, S. Minucci, K.A.M. Abouzid, Surmounting the resistance against EGFR inhibitors through the development of thieno[2,3-d]pyrimidine-based dual EGFR/HER2 inhibitors, Eur. J. Med. Chem. 155 (2018) 316–336.
[60] S.R. Abd El Hadi, D.S. Lasheen, M.A. Hassan, K.A.M. Abouzid, Design and synthesis of 4-anilinothieno[2,3-d]pyrimidine-based compounds as dual EGFR/HER-2 inhibitors 349 (2016) 827–847.
[61] C.H. Wu, M.S. Coumar, C.Y. Chu, W.H. Lin, Y.R. Chen, C.T. Chen, H.Y. Shiao, S. Rafi, S.Y. Wang, H. Hsu, C.H. Chen, C.Y. Chang, T.Y. Chang, T.W. Lien, M.Y. Fang, K.C. Yeh, C.P. Chen, T.K. Yeh, S.H. Hsieh, J.T. Hsu, C.C. Liao, Y.S. Chao, H.P. Hsieh, Design and synthesis of tetrahydropyridothieno[2,3-d]pyrimidine scaffold based epidermal growth factor receptor (EGFR) kinase inhibitors: the role of side chain chirality and Michael acceptor group for maximal potency, J. Med. Chem. 53 (2010) 7316–7326.
[62] D. Kuhn, Targeting Protein Kinases for Cancer Therapy. By David J. Matthews and Mary E. Gerritsen 5 (2010) 1948–1949.
[63] P. Traxler, P. Furet, Strategies toward the design of novel and selective protein tyrosine kinase inhibitors, Pharmacol. Ther. 82 (1999) 195–206.
[64] V.K. Sharma, P.P. Nandekar, A. Sangamwar, H. Pérez-Sánchez, S.M. Agarwal, Structure guided design and binding analysis of EGFR inhibiting analogues of erlotinib and AEE788 using ensemble docking, molecular dynamics and MM-GBSA, RSC Adv. 6 (2016) 65725–65735.
[65] K. Gewald, E. Schinke, H. Böttcher, Heterocyclen aus CH-aciden Nitrilen, VIII. 2-Amino-thiophene aus methylenaktiven Nitrilen, Carbonylverbindungen und Schwefel 99 (1966) 94–100.
[66] V.J. Ram, Thieno[2,3-d]pyrimidines as potential chemotherapeutic agents, Arch. Pharm. 312 (1979) 19–25.
[67] M.E. Azab, H.M.F. Madkour, M.A.E. Ibraheem, Bulgarian, Chem. Commun. 41 (2009) 12–18.
[68] J. van Meerloo, G.J. Kaspers, J. Cloos, Cell sensitivity assays: the MTT assay, Methods Mol. Biol. (Clifton, N.J.) 731 (2011) 237–245.
[69] A. Huether, M. Höpfner, V. Baradari, D. Schuppan, H. Scherübl, EGFR blockade by cetuximab alone or as combination therapy for growth control of hepatocellular cancer, Biochem. Pharmacol. 70 (2005) 1568–1578.
[70] P. Li, Q. Zhang, A. Torossian, Z.-B. Li, W.-C. Xu, B. Lu, S. Fu, Simultaneous inhibition of EGFR and PI3K enhances radiosensitivity in human breast cancer, Int. J. Radiat. Oncol.*Biol.*Phys. 83 (2012) e391–e397.
[71] X. Zhang, H. Nagahara, K. Mimori, H. Inoue, T. Sawada, M. Ohira, K. Hirakawa, M. Mori, Mutations of epidermal growth factor receptor in colon cancer indicate susceptibility or resistance to gefitinib, Oncol. Rep. 19 (2008) 1541–1544.
[72] Y. Zhang, X. Li, X. Xu, W.-J. Luo, Construction of a high-EGFR expression cell line and its biological properties comparing with A431 cell, 2010.
[73] I. Vermes, C. Haanen, H. Steffens-Nakken, C. Reutellingsperger, A novel assay for apoptosis Flow cytometric detection of phosphatidylserine expression on early apoptotic cells using fluorescein labelled Annexin V, J. Immunol. Methods 184 (1995) 39–51.
[74] A. Huether, M. Höpfner, A.P. Sutter, D. Schuppan, H. Scherübl, Erlotinib induces cell cycle arrest and apoptosis in hepatocellular cancer cells and enhances chemosensitivity towards cytostatics, J. Hepatol. 43 (2005) 661–669.
[75] Jin H. Park, Y. Liu, Mark A. Lemmon, R. Radhakrishnan, Erlotinib binds both inactive and active conformations of the EGFR tyrosine kinase domain, Biochem. J 448 (2012) 417.
[76] J. Zhang, P.L. Yang, N.S. Gray, Targeting cancer with small molecule kinase inhibitors, Nat. Rev. Cancer 9 (2009) 28.
[77] R.K. Gill, H. Singh, T. Raj, A. Sharma, G. Singh, J. Bariwal, 4-Substituted thieno[2,3-*d*]pyrimidines as potent antibacterial agents: rational design, microwave-assisted synthesis, biological evaluation and molecular docking studies, Chem. Biol. Drug Des. 90 (2017) 1115–1121.